

Chapter 11. Soil fluxes

Soil is a special natural body, distinct from other rocks...

V.V. Dokuchayev (quoted by V. Vernadsky 1938)

In one of his influential essays on the nature of the biosphere, which subsequently laid the foundation for modern biogeochemistry, Vladimir Vernadsky quoted his geology teacher, Vasily Dokuchayev, in a manner that made clear Dokuchayev's view that soil is uniquely influenced by the organisms that live within; it lies at the interface between geology and biology. Roots and microorganisms exchange materials with the soil and in doing so influence its chemical composition and physical structure. The interactions between the biological and geological components of soil ultimately determine how it interacts with the atmosphere. Soil is the medium through which terrestrial plants gain access to most mineral elements of the geosphere (carbon being the principal exception), and to liquid water from the hydrosphere, both of which influence the capacity for plants to exchange CO₂ with the atmosphere. Microbial activities in soil carry out the recycling of organic matter, returning carbon to the atmosphere; thus closing the terrestrial carbon cycle. Transpiration from plant leaves and evaporation from the soil provide the conduits for water vapor to be exchanged between ecosystems and the atmosphere; thus closing the terrestrial water cycle. Any concentrated consideration of ecosystem-atmosphere exchange must include soil processes in order to fully comprehend the relevant mass and energy fluxes.

Soil is the source of a broad range of trace gases, including CO₂, H₂O, CH₄ and various nitrogen oxide compounds (NO_x). Many of these fluxes originate from plant and microorganism metabolism though, in the case of H₂O, evaporation represents the dominant soil flux. In this chapter, we consider the various biophysical processes that control the exchange of these trace gases between ecosystems and the atmosphere. We begin the chapter with an introduction into soil structure and composition. Discussion of this topic is somewhat limited, with most of the emphasis on the topic of soil organic matter – the principal substrate for soil respiration. We then take up the topic of transport mechanisms for the exchange of mass between soils and the

atmosphere, once again emphasizing the flux of CO₂ from soil respiration. Here, we emphasize the combined contributions of diffusion and bulk flow. In a section on soil evaporation, we consider the driving forces behind latent heat exchange, and derive the most commonly-used model, the Penman equation, for describing evaporative fluxes. Finally, in a series of sections we consider recent observations and models that focus on biological controls over the exchanges of CO₂, CH₄ and NO_x between soils and the atmosphere. Cumulatively, these trace gases represent major contributions to the terrestrial carbon and nitrogen budgets, and in the case of CH₄ and NO_x, major contributions to the reactive photochemistry that occurs in the atmosphere.

11.A. Soil structure and composition

Soils begin as the weathered products of mineral parent materials. Both chemical and physical weatherings contribute to soil formation. Organisms modify the soil even further. They physically fracture rock and soil particles, contribute organic material as excretions when alive and body matter when dead, and modify the physical environment in ways that promote or retard further weathering. Thus, mature soils reflect a complex material with properties of both the parent material and accumulated organic matter. Soils are often described by a taxonomy system based on *horizons*, or layers, classified according to depth, and physical, geological and biological attributes. As soils develop through the continual addition of organic material to the upper layers, and continual addition of parent material to the lower layers, the nature of horizons will change over time. Proper geophysical and geochemical description of soils would require that attention be given to their mineral, or clay, horizons (often designated as the B, C and higher alphabetically-designated horizons). We don't have the luxury of space to do justice to this topic, and its relevance to soil trace gas emissions is less than that for organic matter near the soil surface. Accordingly, we will focus this introductory section on soil organic matter. The organic layers are typically designated as the O (for organic) and A horizons. The uppermost soil horizon, containing recently deposited organic detritus, is the O horizon. The A horizon, located immediately below the O horizon, is often referred to as 'top-soil'.

Soil organic matter (SOM) originates from the leaf and root 'litter' shed by plants, the excrement produced by animals and the recently living, but now dead, bodies of plants and animals. Once litter reaches the soil a series of biological, chemical and photochemical processes begin to decompose it to progressively smaller fragments, and transform it into

alternative chemical forms. *Decomposition* refers to the breakdown of SOM. Decomposition is an ecological 'recycling' process that converts organically bound nutrient elements (such as nitrogen and phosphorus) into inorganic forms, capable of re-assimilation by plants and, at the same time, releases CO₂ back to the atmosphere. In some ecosystems decomposition is initiated while tissues are still attached to living plants, principally through the abiotic photodegradative action of ultraviolet light (Box 11.1). Once tissues are deposited to the soil, photodegradation and biotic degradation, the latter due to microorganisms, act in parallel to decompose the material. An additional process in soil decomposition involves an active set of extracellular chemical reactions that transform SOM molecules into 'stable' polymeric forms, collectively called *humus*. Humus has lost all visible features that might be used to trace it to its original litter source. Soil scientists categorize humus as a mixture of polymers designated as fulvic acid, humic acid or humin depending on acid/base solubility. The production of humus is catalyzed by extracellular enzymes secreted by fungi and bacteria, along with a complex series of uncatalyzed extracellular reactions. As humus is progressively processed through this series of reactions, it is transformed into large supramolecular complexes that are less accessible to microbial degradation, and thus exhibit potentially long turnover times. When considered as a single entity, soil organic matter actually consists of a diverse array of compounds with differing potential to support further decomposition. Some compounds are relatively 'labile' and exist as readily-used substrates for microbial metabolism, whereas others are 'recalcitrant' and remain largely unavailable as microbial substrates. Given that the soil flux of several trace gases to the atmosphere depends on microbial decomposition, the relative distribution of soil organic matter among pools with different turnover potential has a large effect on soil-atmosphere exchange (for a thorough review of decomposition see Berg and McClaugherty 2003).

Mathematical modelers of decomposition processes originally treated the SOM pool as a single entity with exponential decay. As more insight into the decomposition process became available models began to reflect SOM as a composite of discrete fractions that turnover at different rates (e.g., Jenkinson and Rayner 1977, vanVeen and Paul 1981, Parton et al. 1988, Rastetter et al. 1991, Moorhead et al. 1996). Thus, we can identify an 'active' pool having a turnover time ranging from several days to a few years, a 'slow' pool having a turnover time of 20-50 years, and a 'passive' pool that is highly resistant to decomposition with turnover times of 400 to several thousand years (Davidson et al. 2000, Trumbore 2000). The differential age of

these pools is controlled to large extent by differing ratios of ‘labile’ organic compounds, such as sugars and amino acids, to ‘recalcitrant’ organic compounds, such as lignin and complex humic acid polymers. These hypothetical, modeled pools correspond roughly to actual compounds extracted from soils, which can be partitioned into ‘readily soluble’, ‘acid soluble’ and ‘acid insoluble’ fractions. Using the assumption that turnover rate in these pools is correlated with the loss rate of CO₂ to the atmosphere, along with other trace gases, we can begin to couple active soil biogeochemistry with ecosystem-atmosphere exchange.

11.B Scalar diffusion and advection in soils

For the purposes of quantitative flux modeling, soils are considered *porous media*, meaning that the gaseous constituents diffuse through open pores (collectively quantified according to the *soil porosity*) which are interconnected to form transport channels (summarily quantified according to the *soil tortuosity*). The presence of a soil reduces the diffusion coefficient for gases (K_{ds}), relative to the free diffusion coefficient (K_d). The reduction in K_d must occur because soil particles block the shortest path for diffusion of a gas-phase constituent; thus increasing the diffusive path length. With this relation in mind, we can write:

$$K_{ds} = \zeta K_d \quad (11.1)$$

where ζ is the tortuosity coefficient, which scales between 0 and 1. The quantification of ζ in relation to pore size, distribution and shape is difficult. It is more common to use an empirical relation that relates ζ to soil air space volume (f_a), which is in turn a function of soil density, an easily measured property of soils. The soil air space volume (f_a) is the ratio of air-filled pore volume to total soil volume (m³ m⁻³). Empirical relations that have been used in the past to define ζ include:

$$\begin{aligned} \zeta &= 0.66 f_a && \text{Penman (1940)} \\ \zeta &= f_a^{1.5} && \text{Marshall (1959)} \\ \zeta &= \frac{f_a^{(10/3)}}{\Phi^2} && \text{Millington and Quirk (1961)} \quad (11.2) \\ \zeta &= (2f_{a100}^3 + 0.04f_{a100}) \left(\frac{f_a}{f_{a100}} \right)^{2+3/b} && \text{Moldrup et al. (2000)} \end{aligned}$$

where total soil porosity (Φ) is defined as total pore volume per unit soil volume ($\text{m}^3 \text{m}^{-3}$), the parameter f_{a100} is a standardized measure of air-filled pore volume determined empirically at a soil-water pressure head of -100 cm of water, and b is the Campbell moisture retention function which is determined empirically according to Campbell (1974). There have been efforts to use the theory of fractal shape and distribution to define aspects of soil porosity (e.g., Rieu and Sposito 1991, Bird et al. 2000), and these approaches may lead to improved modeling of ζ in the future; at present, however, they remain highly conditioned on empirical relations, and in that regard they are no better than the existing models discussed above. Using the relations shown in Equation 6.2, the steady-state diffusive flux of molecules through soil can be represented as:

$$F_d = -K_{ds} \left(\frac{\partial c}{\partial x} \right) \quad (11.3).$$

In the presence of wind, gas fluxes from the soil surface are driven by mass flow along pressure gradients, in addition to diffusion (Takle et al. 2004). The flux due to mass flow is called an *advective flux*. Within-soil advective fluxes are often caused by *pressure pumping*. Pressure pumping occurs because of small irregularities in the topography of the surface which induce changes in the speed and angle of wind flow and cause heterogeneous momentum transfer across the surface (Fig. 11.1). Local differences in momentum transfer will, in turn, cause fluctuations in the near-surface pressure field, creating pulses or waves of air. Models that have attempted to incorporate pressure pumping into predictions of soil trace gas fluxes begin with wave-like transmission of a fluctuating pressure field into the soil (see Massman 2006). Once transmission of the pressure field has been resolved, Darcy's Law is used to relate the advective flux of gas-phase constituent j (F_{aj}) to gradients in pressure:

$$F_{aj} = -\frac{k_a}{\mu} \rho_a c_j \nabla p \quad (11.4)$$

where F_{aj} carries units of $\text{kg m}^{-1} \text{s}^{-1}$, k_a is air permeability of the soil with units m^2 , μ is dynamic viscosity of air with units $\text{kg m}^{-1} \text{s}^{-1}$, ρ_a is mean air density (kg m^{-3}), c_j is mole fraction of

constituent j , and p is pressure with units $\text{kg m}^{-1} \text{s}^{-2}$ ($= \text{Pa}$). The symbol ∇ is the gradient operator for pressure; with:

$$\nabla p = \frac{\partial p_x}{\partial x} + \frac{\partial p_y}{\partial y} + \frac{\partial p_z}{\partial z} = \frac{\partial p_i}{\partial x_i} \quad (11.5)$$

(See the Mathematical Supplement at the end of the book for further discussion on gradient operators.) The total flux of constituent j within the soil pore channels can be described as the sum of the diffusive and advective fluxes ($F_j = F_{dj} + F_{aj}$):

$$F_j = F_{dj} + F_{aj} = -K_{ds} \rho_a \nabla c_j + \frac{k_a}{\mu} \rho_a c_j \nabla p \quad (11.6)$$

11.C Soil evaporation

Water is transported from ecosystems to the atmosphere through the parallel fluxes of soil evaporation and plant transpiration; together we refer to these fluxes as *evapotranspiration* (ET). We considered the processes associated with transpiration in Chapter 7. Here, we take up the topic of *soil evaporation*. If we begin from the condition of a wet surface, we can equate the driving and resistive forces of evaporation to those that exist for an open pan of water. Radiant energy from the sun and sky, sensible heat from the atmosphere, or stored heat conducted up through the soil, is absorbed by the surface, and some fraction of that energy will be used to evaporate water. The evaporative flux of H_2O will be mitigated by the resistive tendency of still air next to the surface, the so-called *surface boundary layer*. The thickness of the boundary layer, and thus the extent of the resistance, will depend on wind speed and surface roughness. In the case of a 'wet' soil surface, the structural and compositional properties of the soil have little influence over the evaporative flux; the principal controls are found in the rate of energy absorption and the thickness of the boundary layer.

However, the soil surface is seldom truly 'wet'. In the absence of perennial moisture inputs, the soil will dry and the evaporation front, or effective evaporation surface, will migrate to deeper soil layers. As the evaporation front moves deeper, water molecules that enter the vapor phase must cross 'dry' surface layers, moving through air-filled pores and channels. In this

unsaturated condition, soil structure and composition exert greater control over the rate of evaporation. As we develop the modeling framework for soil evaporation we will first consider the case of a 'wet' soil surface, followed by the case of a 'dry' (unsaturated) soil.

Description of the evaporative flux from a wet soil generally begins with the Penman equation (Penman 1948) (see Chapter 5):

$$\lambda_w E = \underbrace{\frac{s}{s + \gamma} (R_n - G)}_{\text{Term I}} + \underbrace{\frac{\gamma}{s + \gamma} \lambda_w E_a}_{\text{Term II}} \quad (11.7)$$

where λ_w is the latent heat of vaporization for water ($\text{J mol}^{-1} \text{H}_2\text{O}$), E is the evaporation rate ($\text{mol H}_2\text{O m}^{-2} \text{s}^{-1}$), s is the slope of the relationship between saturation water vapor mole fraction and air temperature ($\text{mol H}_2\text{O mol}^{-1} \text{air K}^{-1}$), γ is the psychrometer constant ($\text{mol H}_2\text{O mol}^{-1} \text{air K}^{-1}$) ($\gamma = c_p/\lambda_w$ where c_p is the specific heat of dry air in units of $\text{J mol}^{-1} \text{air K}^{-1}$), R_n is net radiation ($\text{J m}^{-2} \text{s}^{-1}$), G is the heat flux conducted from the soil surface to deeper layers in the soil (i.e., not available for surface evaporation) ($\text{J m}^{-2} \text{s}^{-1}$), and E_a is the evaporative flux. E_a can be described according to a diffusive analog model scaled to the difference in water vapor concentration between air next to the surface and that in the well-mixed atmosphere above the surface:

$$E_a = \rho_a (c_{wa}^* - c_{wa}) f(U) \quad (11.8)$$

where ρ_a is the molar density of dry air (mol air m^{-3}), c_{wa}^* is the saturation mole fraction of water vapor in air at the surface ($\text{mol H}_2\text{O mol}^{-1} \text{air}$), c_{wa} is the mole fraction of water vapor in the atmosphere above the surface, and U is wind speed (m s^{-1}). The Penman equation combines the controls over evaporation rate by the surface energy budget (Term 1) and the water vapor concentration gradient (Term 2). Since its original derivation, the Penman equation has been modified to place the theory within the context of fundamental transport resistances, rather than relying on empirical functions related to windspeed. Thus, the most commonly-used model to predict evaporation from 'wet' surfaces in more recent decades has been the Penman-Monteith equation:

$$\lambda_w E = \underbrace{\frac{s}{s + \gamma^*} (R_n - G)}_{\text{Term I}} + \underbrace{\frac{\rho_a c_p (c_{wa}^* - c_{wa})}{(s + \gamma^*) r_H}}_{\text{Term II}} \quad (11.9)$$

where γ^* is a modified psychrometer constant that takes into account the differential effect of aerodynamic processes on the transport resistances of heat and water vapor ($\gamma^* = \gamma r_w / r_H$, where r_w and r_H are the aerodynamic resistances to heat and water vapor transport, respectively, with units $s m^{-1}$). The Penman-Monteith equation includes the implicit assumption that resistances to heat and water vapor transport can be described by Ohm's Law analog terms (r_H and r_w), a concept more appropriately applied to diffusive fluxes, than aerodynamic fluxes. Thus, some caution must be applied to interpretation of the resistance terms in Equation 11.9. More fundamental treatments of the Penman and Penman-Monteith equations are presented in Chapter 5.

As the evaporation front moves deeper into an unsaturated soil, soil factors, such as the transport resistance of relatively dry upper soil layers, must be considered in addition to atmospheric factors. Most past models of soil evaporation rate in unsaturated soils have focused on diffusive-analog equations, which lend themselves to clear development of transport resistance as a dominant controlling factor. Two of the more general forms are:

$$E = \frac{P}{RT} \frac{(\alpha c_{wa}^* - c_{wa})}{r_w} \text{ or } E = \frac{P}{RT} \beta \frac{(c_{wa}^* - c_{wa})}{r_w} \quad (11.10)$$

where E is soil evaporation rate ($\text{mol H}_2\text{O m}^{-2} \text{ s}^{-1}$), P is atmospheric pressure (Pa), R is the universal gas constant ($\text{m}^3 \text{ Pa mol}^{-1} \text{ K}^{-1}$), T is temperature (K), c_{wa}^* is the saturation mole fraction of water vapor at the temperature of the surface ($\text{mol H}_2\text{O mol}^{-1} \text{ air}$), c_{wa} is the mole fraction of water vapor in the atmosphere above the surface, r_w is the aerodynamic resistance ($s m^{-1}$) associated with the atmospheric transport of H_2O vapor, and α and β are coefficients that modify the diffusive driving force or the relative influences of atmosphere versus soil as transport resistances, respectively. These two equations are sometimes referred to as the α and β evaporation models, respectively. The term α is defined as the fractional relative humidity of the air in unsaturated soil pore spaces that is in equilibrium with the matric potential of the soil:

$$\alpha = \exp \frac{\Psi_m \bar{V}_w}{RT} \quad (11.11)$$

where Ψ_m is matric potential (MPa) (see Section 5.D) and \bar{V}_m is the partial molal volume of water ($\text{m}^3 \text{mol}^{-1}$). As the soil dries, water in the soil pores will retreat and concavities will develop at air-water interfaces, reflecting increased surface tension. The increased surface tension represents a force that resists the diffusion of water molecules from the liquid phase to the vapor phase in the soil air spaces, and therefore decreases soil air humidity. It is unlikely that matric potential becomes a significant factor controlling evaporation rates until the relative humidity in the soil air spaces decreases to below 80-85%; at which point the free energy of water vapor in the soil air spaces potentially decreases below that of water films held to soil particles by matric forces. The term β is defined as the ratio of r_w to the sum of r_w plus the soil resistance to H_2O diffusion through the soil air spaces to the soil surface (r_s):

$$\beta = \frac{r_w}{r_w + r_s} \quad (11.12)$$

By incorporating β into the model of Equation 11.10, the overall transport resistance can be scaled to reflect greater or lesser control by atmospheric processes.

Modeling of the transport resistances in unsaturated soil is complex, and considerable work is required before we can cast these models in more fundamental terms. Thermal gradients, and their effect on both liquid and vapor transport, are not well represented in the current models. Heating of the surface, for example, causes water vapor gradients to develop in the downward direction, forcing diffusion and bulk flow to occur from shallower layers to deeper layers. In contrast, convective cooling of the surface may cause a reversed gradient, supporting water vapor transport from deeper layers to shallower layers. The redistribution of water in soils, as a result of thermal gradients can, in turn, influence thermal conductivity; thus, there are complex direct interactions and feedbacks to resolve before we can understand the coupling of heat and water transport in unsaturated soils. Temperature can affect liquid water through influences on both viscosity and surface tension, which in turn can influence capillarity in soil pores and

channels. None of these temperature effects are adequately described in the current generation of soil moisture models.

As an alternative to the mechanistic approach provided by numerical models, some analytical models for soil water transport have also been proposed. One such model was developed by Chanzy and Bruckler (1993):

$$\frac{E_a}{E_p} = \left[\frac{\exp(A\theta + B)}{1 + \exp(A\theta + B)} \right] C + (1 - C) \quad (11.13)$$

where E_a is the actual daily evaporation rate, E_p is the potential daily evaporation rate, θ is the integrated soil moisture content ($\text{m}^3 \text{H}_2\text{O m}^{-3}$ soil) in the upper 5 cm of soil, and A , B and C are soil-specific coefficients. The coefficients A , B and C are defined according to:

$$\begin{aligned} A &= a + 5 \max \{3 - E_p, 0\} \\ B &= b - 5 \max \{3 - E_p, 0\} \\ C &= 0.9 - 0.05 c (U_d - 3) \end{aligned} \quad (11.14)$$

where a is a dimensionless coefficient that controls the slope of the daily decrease in θ in an unsaturated soil, b is a dimensionless coefficient that controls the shape of the relation between decrease in θ and time across days, c is a coefficient (s m^{-1}) that controls the sensitivity of E_a/E_p to wind speed, and U_d is the daily integrated horizontal (advective) wind speed (m s^{-1}) (Table 11.1). E_p is typically derived from the Penman equation. Thus, the Chanzy-Bruckler model relates actual to potential evaporation depending on soil moisture content, time since wetting, and weather (which is integrated into factors such as wind speed and rates of drying).

11.D Soil respiration

Soil respiration represents a major component of ecosystem and global carbon budgets and, because of its high sensitivity to temperature, it is potentially one of the principal determinants of the ecosystem responses to climate change (Raich and Schlesinger 1992, Raich and Potter 1995). Unlike cellular respiration, soil respiration reflects a combination of processes from different organisms, including plants, fungi and microbes. These separate components of soil respiration

are referred to by different names (e.g., autotrophic versus heterotrophic, root versus microbial); in this book they will be referred to as the *rhizospheric* versus *decomposition* fractions (Fig. 11.2). The rhizospheric fraction is due to a diverse group of organisms, including mycorrhizal fungi, rhizospheric bacteria and plant roots, all of which share the property of being dependent on the downward transport of carbohydrates and other nutrients from autotrophic shoots (often called *rhizodeposition*; see Paterson 2003). The decomposition fraction is due to the CO₂ loss from heterotrophic microorganisms as they decompose soil organic matter. Some past studies have used various experimental approaches to partition and quantify the relative contributions from the rhizospheric and decomposition fractions. In one innovative approach, plants are 'girdled' by cutting a swath of phloem tissue (and bark) away from the stem, which effectively eliminates rhizodeposition. Experiments of this type have revealed that the rhizospheric fraction represents 40-60% of the total soil respiration rate in several forest ecosystems, with the rest being due to decomposition (Högberg et al. 2001, 2009, Scott-Denton et al. 2005).

11.D.1 Substrate controls on soil respiration

The rate of heterotrophic decomposition in a particular soil is dependent on interactions between the substrate quantity and quality, climate, and the types of microorganisms present in the soil. These factors are not completely independent of one another. Substrate quantity and quality will be to a large extent dependent on the types of plants that occupy the site, which is determined in part by climate, and the nature of the organic matter substrates will be altered by the progressive action of decomposer communities. Decomposer communities, in turn will reflect available substrate quality and quantity and they will change as the nature of the substrate changes in response to progressive decomposition. Thus, there are tight connections and feedbacks among these controlling factors.

By definition, the active soil organic matter pool will be the one most readily utilized by soil decomposers, followed by the slow and passive pools, respectively. Each of these pools is associated with a unique 'guild' of decomposer organisms. The initial decomposition process is most often conducted by extracellular enzymes produced by the decomposer microbes (Burns and Dick 2002). These enzymes can either be attached to the outer cell wall surface of the microbes or completely free in the soil medium. Extracellular enzymes are responsible for the

initial depolymerization of complex SOM substrates and production of smaller molecules that can be assimilated and metabolized by microbial cells.

The rate of SOM decomposition is observed to increase in many ecosystems as the result of *substrate priming*. Priming occurs when the addition of organic substrates to a soil stimulates the rate of decomposition of both the added substrate and previously existing substrates. Priming may involve the production of new extracellular enzymes (Kuzyakov et al. 2000, Subke et al. 2004, Weintraub et al. 2007) and changes in microbial community composition (Waldrop and Firestone 2004). Priming represents an amplification of the soil respiration rates as a result of the addition of new substrates. This effect has not been included in most soil respiration models.

The details of the taxonomic composition of different decomposer guilds, and the types of extracellular enzymes produced by them, are not well known. We know that the relations between decomposer respiration rate and climate varies among different soils suggesting that the differential nature of substrates and affiliated decomposer communities matters when it comes to predicting dynamics in soil respiration. Molecular identification techniques are being applied to studies of soil microbial communities progressively more frequently, so it is likely that we will learn much more about specific substrate-microbe interactions in the future. In the meantime, modeling efforts have proceeded with the assumption that microbial guilds from each SOM substrate pool will impose different kinetic constraints on the rate of respiratory CO₂ production, and a framework for testing these assumptions exists (see Box 11.2).

11.D.2 Climate controls on soil respiration

The Q_{10} for soil respiration rate is a principal parameter in the analysis and modeling of ecosystem and global carbon budgets (Raich and Potter 1995) (see section 4.D.2). Q_{10} values ranging from 1.5 to 3.5 have been used to describe the temperature-dependence of soil respiration and, in general, the models that have been applied to plant tissue respiration also work well for describing soil respiration (Lloyd and Taylor 1994, Fang and Moncrieff 2001). The temperature response of soil respiration rate, however, is controlled by complex interactions involving root densities and levels of metabolic activity, the availability and nature of the soil organic carbon pools (Kirschbaum 1995, Trumbore et al. 1996, Giardina and Ryan 2000, Fang and Moncrieff 2005) and seasonal temperature acclimation (Luo et al. 2001). It is likely that temperature (and precipitation) affects the rhizospheric and decomposition fractions of soil

respiration differently (e.g., Scott-Denton et al. 2006). However, our ability to characterize these differences in quantitative models is limited.

Past studies have revealed contrasting conclusions about the relationship between temperature and soil respiration rate. In a meta-analysis of studies on soil respiration from a range of sites across a broad latitudinal gradient, Giardina and Ryan (2000) concluded that substrate quality, rather than temperature, was the primary determinant of soil respiration rate. This conclusion was in contrast to those drawn from other studies in which temperature was shown to be the most important control over geographic patterns in soil respiration (Davidson et al. 2000, Trumbore 2000). In a study meant to reconcile these differences, Knorr et al. (2005) showed that temperature can exert a dominant influence on soil respiration rate if one considers differences in the temperature dependencies of different substrate pools. To illustrate this reconciliation consider two sites, one with a warmer climate than the other. If the SOM substrate pool at the warmer site is smaller and composed of more labile compounds, compared to the cooler site, then incubations of soil from each site (which often last for months) at their respective mean temperatures will potentially yield similar amounts of respired CO₂. This observation may lead to the conclusion that soil respiration is relatively insensitive to temperature. However, the total amount of CO₂ produced from soil of the warmer site may have been limited by the smaller amount of labile substrate which was oxidized at higher rates in the face of warmer temperature. Slower decomposition of the SOM substrate from the cooler site may have been compensated by a larger substrate pool, resulting in total CO₂ production equal to that of the warmer site (Figure 11.3). The lesson from this study is that it's the interaction of temperature and substrate pool that determines the ultimate rate of CO₂ production. The relations among temperature, substrate and soil respiration rate are further complicated by evidence that older, more recalcitrant SOM pools have higher intrinsic sensitivities to temperature than younger, more labile pools (Knorr et al. 2005, Huntley and Ineson 2008), and that multiple processes interact to determine these sensitivities (Agrem and Wetterstedt 2007, Gershenson et al. 2009). Until our understanding of these complex interactions improves, assumptions about the generality of the temperature dependence of soil respiration must carry significant uncertainty.

Soil moisture content also exerts an important control over soil respiration rate. Bacteria and fungi are dependent on the thin film of water that surrounds soil particles to maintain

favorable hydration and facilitate the diffusion of substrates through the soil medium (Borken and Matzner 2009). Soil drying can force changes in microbial metabolism, accelerate cell death and thus generally alter the availability of organic substrates. Microbial death during drought produces organic matter that can persist in the soil and serve as the substrate for growth of a new generation of microbes that arises upon re-wetting. Soil moisture content can also influence the physical nature of soil. For example, in many soils the uppermost organic horizon layer tends to be hydrophobic; intact leaf fragments and microbially-processed polymers from the initial phases of decomposition are often composed of hydrophobic compounds (Doerr et al. 2007). Hydrophobicity of the upper soil horizon often increases during drought. Thus, when precipitation occurs following a prolonged drought, penetration into the soil may be limited. Water from rain events that does make it into the soil can potentially displace air within soil pores and flush stored CO₂ in large pulses. This CO₂ is decoupled in time from the respiratory process that produced it. Following the initial flush of CO₂ due to displacement by water, soil microorganisms can respond quickly and positively (within 1-2 days) to the moisture pulse, growing on the remains of the previous generation and causing sustained increases in soil CO₂ fluxes (Liu et al. 2002).

11.D.3 Models of soil respiration

Efforts to understand and quantify soil respiratory CO₂ fluxes have increased in frequency over the past couple of decades due principally to recognition of the high sensitivity of the soil CO₂ flux to climate change. Most efforts have focused on interactions between climate and substrate as controls over the decomposition component of soil respiration, and climate as a control over the rhizospheric component (Fig. 11.4). At the most fundamental level, the size of the pool of SOM that supports decomposition respiration is controlled by mass balance constraints, reflecting the relative rates of litter input (linked to NPP) and CO₂ output (linked to microbial biomass) (Fig. 11.5). The size of the photosynthate pool that supports rhizospheric respiration is also correlated NPP, and output of CO₂ as the photosynthate is oxidized during rhizospheric metabolism reflects root biomass and nutrient uptake activity. These fundamental concepts are often used as the basis for soil respiration models. Ultimately, the soil respiration rate will be constrained at one limit by NPP and at another limit by the rates of microbial and

root metabolism. In this regard it has been noted that there is a positive correlation between annual rates of NPP and soil respiration (Raich and Schlesinger 1992).

Temperature is the climatic variable most commonly used to drive soil respiration models. In part, this is because soil respiration rate is highly sensitive to temperature, temperature is a central driver of ecosystem responses to future climate change, and the Arrhenius model for the temperature sensitivity of biological processes (see Section 4.D.2) is readily accessible as a mathematical starting point. However, simple models that link respiration to temperature, as a means to predict the response of soil respiration to future climate warming are likely to miss important connections to changes in NPP, and thus changes in the potential for substrate to act as an important controlling variable. To illustrate this point, imagine a C_3 ecosystem in a moderate-to-warm climate zone with SOM pools at steady state. This means that the inputs of substrate and outputs of CO_2 are in flux balance. If we now impose an increase in mean annual temperature on the system, we can predict on the basis of the first principles of metabolism that soil respiration rate will increase. However, it is also likely that NPP will decrease due to higher rates of leaf photorespiration. If allowed to achieve a new steady state, in the presence of this temperature increase, the SOM pool should eventually equilibrate with these flux dynamics and settle on a smaller size. It is possible that in the face of smaller the SOM pool, overall control over soil respiration rate will shift to favor substrate supply, rather than temperature. Now, imagine that the imposed temperature increase is accompanied by an increase in atmospheric CO_2 concentration. The higher CO_2 concentration should alleviate, to some extent, the effect of the higher temperature on photorespiration, and thus offset the decrease in NPP. If SOM substrate supply is in the range that limits the rate of soil respiration, then higher NPP will potentially support increases in both the substrate pool size and soil respiration rate, with both eventually reaching new steady values. If substrate supply is high enough not to limit the respiration rate, but rather climate exhibits the dominant limiting control, then the increase in NPP will cause an increase in substrate pool size, but no increase in the steady-state soil respiration rate. Consideration of these complex interactions is a good exercise for students to consider, as it puts into practice some of the fundamental principles in metabolism and mass balance that we have discussed in previous chapters. However, it also illustrates the importance of quantitative models as tools to resolve the complexities of interactions and feedbacks.

11.D.4 The isotopic influence of soil respiration on atmospheric CO₂

The isotopic composition of atmospheric CO₂ has become a valuable diagnostic metric by which to evaluate the relative influences of plant and soil fluxes on atmospheric CO₂ concentration. During a single day and immediately above an ecosystem, photosynthetic CO₂ assimilation by plants causes enrichment of atmospheric ¹³CO₂, in the daylight hours, but depletion at night.¹ This diurnal pattern is due to the fact that Rubisco, the principal carboxylating enzyme of C₃ photosynthesis, assimilates ¹²CO₂ at a greater rate than ¹³CO₂ during the day (see Section 3.D), but soil respiration, using organic substrates depleted in ¹³C, adds CO₂ back to the atmosphere at night. Thus, the use of recently-assimilated photosynthetic products as substrates for soil respiration provides a connection in the fluxes of CO₂ entering and exiting the ecosystem. Theoretically, if the photosynthetic and respiratory CO₂ fluxes were completely coupled at the diurnal time scale (i.e., if the photosynthetic products cycled through the rhizospheric and decomposition components of soil respiration within the same day) then the mean diurnal ¹³C/¹²C of the near-canopy atmosphere ($\bar{\delta}_a$) should not change. This condition can be stated formally as:

$$\int_0^{24\text{h}} \frac{d\bar{\delta}_a}{dt} dt = 0 = \delta_A F_{cA} + \delta_R F_{cR} = (\bar{\delta}_a - \Delta_c) F_{cA} + \delta_R F_{cR} \quad (11.15)$$

where δ_A represents the ¹³C/¹²C ratio of the photosynthetic products provided by the canopy, F_{cA} is the net photosynthetic flux of the canopy, δ_R is the ¹³C/¹²C ratio of the respired CO₂ from heterotrophic components of the ecosystem (including soil microbes, roots, stems and branches), F_{cR} is the ecosystem respiratory flux, and Δ_c is the photosynthetic discrimination against ¹³C provided by the canopy. In essence, Equation 11.15 states the condition of diurnal *isotopic equilibrium* between the photosynthetic and respiratory components of the ecosystem.

Isotopic equilibrium is not achieved in real ecosystems. This is due to the fact a unit mass of CO₂ that is photosynthetically removed from the atmosphere at one isotope ratio in any single day is replaced by a unit mass of respired CO₂ that exists at a different isotope ratio. The result is *isotopic disequilibrium*. The isotopic ratio of CO₂ produced through soil respiration is affected by the age of SOM pools that serve as substrates. Recall that SOM in the 'slow' and 'passive' pools is tens to thousands of years old. Much of the carbon in these pools was assimilated from

the atmosphere prior to the Industrial Revolution; prior to the large-scale emission of fossilized carbon from coal and oil with inherently low $^{13}\text{C}/^{12}\text{C}$ ratios. Because of these emissions, the isotopic composition of the atmosphere has changed. The use of respiratory substrates from 'old' SOM pools will add CO_2 to the atmosphere that is at isotopic disequilibrium with the cycling of carbon through active, 'young' SOM pools. The degree of disequilibrium will be influenced by the relative rates of substrate utilization from the different SOM pools. At disequilibrium the left-side term of Equation 11.15 will not equal 0, and the resulting time-dependent change in the $^{13}\text{CO}_2/^{12}\text{CO}_2$ ratio is called the *disequilibrium flux*. The presence of an isotopic disequilibrium means that the relative concentrations of carbon isotopes in the CO_2 of the atmosphere will change, despite no change in overall CO_2 concentration. The effect of differential oxidation of SOM pools, and its influence on isotopic disequilibrium, must be taken into account for accurate quantification of the effect of soil respiration on the $^{13}\text{CO}_2/^{12}\text{CO}_2$ composition of the atmosphere (Fung et al. 1997). Past efforts have relied on dynamic models of SOM oxidation to provide residence times of each SOM pool, which are then coupled to predicted changes in the $\delta^{13}\text{C}$ ratio of atmospheric CO_2 to provide the disequilibrium flux (Ciais et al. 1999, Scholze et al. 2008).

The concept of isotopic equilibrium is illustrated at the global scale in Figure 11.6. The decrease in the $\delta^{13}\text{C}$ ratio of the atmosphere due to the combustion of fossil fuels over the past two centuries is estimated according to Francey et al. (1999). Over this same time, the $\delta^{13}\text{C}$ ratio of photosynthate would have tracked that of the atmosphere, but with an offset due to photosynthetic discrimination of ~ 18 ‰ (globally averaged and including weighted discrimination by both C_3 and C_4 dominated ecosystems). The change in $\delta^{13}\text{C}$ of the atmospheric CO_2 is lagged by several years due to SOM residence time. In this analysis we have presented two alternative globally-averaged residence times for SOM (τ); 18 years (after Randerson et al. 1999) and 27 years (after Yakir 2004). The effect of a change in estimated residence time is clearly seen as causing an increase in the globally-averaged isotopic disequilibrium; the isotopic disequilibrium with $\tau = 18$ years (D_{18}) is estimated as 0.4 ‰, whereas with $\tau = 27$ years (D_{27}) it is estimated as 0.6 ‰. These values only take into consideration the time lag between CO_2 assimilation and respiration due to the residence of assimilated carbon in SOM.

An additional factor influencing isotopic disequilibrium is the time-dependent enrichment in ^{13}C in SOM during mineralization; this is often observed as a 1-3 ‰ increase in $\delta^{13}\text{C}$ of SOM

as a function of depth in forest soils (Nadelhoffer and Fry 1988) (Fig. 11.7). Deeper SOM is also older, so some of the increase in $\delta^{13}\text{C}$ can be attributed to CO_2 assimilation in a pre-industrial atmosphere. However, this can only account for, at most, $\sim 1.4\%$ of the observed increase. The residual difference is likely due to differences in the isotopic composition of plant biomass versus microbial biomass, and/or microbial discrimination favoring ^{12}C in respired CO_2 (Ehleringer et al. 2000, Torn et al. 2002). Whatever the cause, the heavier isotopic composition of older SOM, above that caused by changes in atmospheric composition alone, will influence atmospheric isotopic disequilibrium as it is oxidized.

An additional isotopic tool that can be used to study the turnover rates of SOM involves the quantification of ^{14}C (Trumbore 2000). In SOM with residence times of centuries to millennia, age can be determined by the rate of radioactive decay of ^{14}C , which exhibits an isotopic half-life of $\sim 5,700$ years. However, ^{14}C abundance can be used in a slightly different way to estimate turnover times for SOM within the past few decades. During the period 1959-1963, ^{14}C was introduced to the atmosphere in significant quantities during relatively frequent aboveground atomic bomb testing. This pulse of ^{14}C was assimilated into the biosphere through photosynthesis and can be used as a natural tracer to estimate carbon compound turnover times as it moves through pools of leaves, litter and SOM (Goh et al. 1976). In the soil of a deciduous oak-maple forest in the northeastern U.S., the ^{14}C content of various SOM pools was used to estimate turnover times of 2-5 years for leaf litter, 5-10 years for root litter, 40-100 years for low-density humified SOM, and > 100 years for mineral-associated SOM (Gaudinski et al. 2000). In the same study, ^{14}C was used to show that CO_2 derived from SOM that was 1 year or greater in age represented $\sim 40\%$ of the annual soil respiration flux.

11.E Methane emissions from soils

Methane (CH_4) is emitted at relatively high rates from wetland soils, the digestive tracts of ruminant animals, and anthropogenic processes concerned with the extraction and transfer of natural gas (Wuebbles and Hayhoe 2002, IPCC 2007). Global emissions of CH_4 have increased from approximately 200 Tg yr^{-1} prior to the Industrial Revolution of the 19th Century, to approximately 500 Tg yr^{-1} at the beginning of the 21st Century (Dlugocenyk et al. 1998, Houweling et al. 2000, Le Mer and Roger 2001). Global soils are likely responsible for 100-200 Tg yr^{-1} of CH_4 emissions (Le Mer and Roger 2001). Soils also take up CH_4 at the global rate of

20-40 Tg yr⁻¹ (Dutaur and Verchot 2007). The production and consumption of CH₄ in soils are due to microbial activities. *Methanogens* are a group of archaea microorganisms that inhabit anaerobic soils and produce CH₄ after transferring energy-rich electrons from organic matter to CO₂, which they use as a terminal electron acceptor (see Section 3.B). *Methanotrophs* are a group of bacteria capable of oxidizing CH₄, which they use as their principal carbon and energy source.

Methanogens produce CH₄ as an end-product of respiratory metabolism in which they oxidize compounds, such as acetate (CH₃COOH) and molecular hydrogen (H₂). The production of CH₄ from the oxidation of these compounds is exemplified in the following pair of reactions:



The anaerobic metabolism of alcohols, fatty acids, amino acids and various aromatic compounds contained in SOM produces the H₂ and CH₃COOH used as initial substrates. The metabolism that produces CH₃COOH and H₂ is endergonic (positive ΔG'₀) whereas the methanogenic oxidation to produce CH₄ is exergonic (negative ΔG'₀), under standard conditions. The only way that the entire metabolic pathway is permissible according to thermodynamics is for methanogenic communities to remove the end-products of the metabolism (CH₃COOH and H₂) at a rate that maintains disequilibrium and allows the metabolism to progress according to mass action. Thus, the various microbial assemblages that produce and consume CH₃COOH and H₂ are forced by thermodynamics into obligatory, cooperative associations. The role of methanogens in these associations was nicely described in a quote by Schink (1999), “although (methanogens) are among the last actors in the (methanogenic) play, they conduct the whole process to a maximum energetic efficiency.”²

Methanotrophs can grow aerobically or anaerobically with CH₄ as their only source of energy and carbon (Anthony 1982). In aerobic methanotrophy CH₄ is oxidized in an initial step to methanol according to:



The methanol produced in Reaction 11.18 is progressively oxidized to formaldehyde, formate and CO₂ by the enzymes methanol dehydrogenase, formaldehyde dehydrogenase and formate dehydrogenase, respectively. The most common methanotrophs belong to the gram-negative eubacteria group of microbes. Because of their specialization on CH₄ as a respiratory substrate, methanotrophs are common in the upper (aerobic) layers of wetland soils where they gain access to CH₄ released by methanogens living in the lower (anaerobic) soil layers (Fig. 11.8A).

The magnitude of CH₄ emissions, and the processes that transport it to the atmosphere, have become of special concern in recent years because of the contribution of increasing atmospheric CH₄ concentrations to climate warming. Methane is approximately twenty times more potent as a greenhouse gas, compared to CO₂. This high potency is mostly due to the lower concentration of CH₄ in the atmosphere, compared to CO₂. In order to understand this relationship we note that when a molecule of a radiatively active trace gas is added to the atmosphere, its capacity to absorb radiation is influenced by the concentration of other molecules that absorb radiation at the same wavelengths. The fact that the existing concentration of CH₄ is nearly two-orders of magnitude lower than that of CO₂ means that each molecule of CH₄ that is added has the potential to more greatly affect radiative warming compared to each molecule of added CO₂. Methane also exerts a dominant control over the oxidizing power of the troposphere because it is reactive with hydroxyl radical (OH), which oxidizes CH₄ to CO, and ultimately CO to CO₂.

11.E.1 Methane transport mechanisms

In wetland ecosystems, CH₄ is transported from the soil to the atmosphere by molecular diffusion, ebullition or bubbling, and transport through plant tissues. Transport through plants accounts for most of the global CH₄ flux (e.g., Holzappel-Pschorn et al. 1986, Kim et al. 1998). The transport of CH₄ through wetland plants is facilitated by *aerenchyma*, a tissue in stems, roots and leaves that is specialized for gas transport (Jackson and Armstrong 1999). Aerenchyma tissue can form from the genetically-programmed separation of cells, creating air spaces between them (*schizogenous aerenchyma*), or from the death of cells with subsequent cell lysis (*lysigenous aerenchyma*). Lysigenous aerenchyma is more common in many of the wetland species that facilitate CH₄ emission. Lysigenous aerenchyma provides tissues with continuous air passages through the length of roots, stems and leaves, allowing for O₂ to diffuse downward

into water-logged soils, and allowing CH₄ to diffuse upward to the atmosphere (Figure 11.8B). The formation of lysigenous aerenchyma is promoted by anaerobiosis. Differences in the tendency to form lysigenous aerenchyma are the cause of CH₄ transport differences among cultivars of rice, for example (Aulakh et al. 2000). In addition to facilitating the upward transport of CH₄, aerenchyma facilitates the downward transport of O₂. This permits a zone of CH₄ oxidation within the rhizosphere next to O₂ emitting roots, and patterns of O₂ deposition to the soil can cause methanotrophic and methanogenic bacteria to become differentially partitioned into zones of CH₄ production and oxidation.

Methane can also be transported through plant tissues by pressurized bulk flow. Pressure gradients can develop in wetland plant systems from a variety of causes, and the belowground rhizome connections among the plants of wetland species can sustain pressure-driven convection.³ In some species, such as those in the genera *Phragmites* and *Typhus*, broken stems, or culms are connected to other broken stems of different heights; this condition can facilitate pressure gradients in a manner similar to the pressure-pumping discussed above for soil advection. Wind speed decreases sharply as the ground is approached. Reduced wind speed at lower heights must be balanced by higher pressure (momentum must be conserved); thus, a pressure gradient exists between the two openings at different heights, potentially facilitating bulk flow through the system (Fig. 11.8C).

Pressure-driven flows in wetland plants can also be caused by thermal- and humidity-induced diffusion (Armstrong et al. 1996). In this case, diffusion sets up the condition for bulk flow. To illustrate, imagine a closed volume of air in contact with an evaporative surface, and separated from the atmosphere by a porous membrane. In this condition, the potential exists for differential pressures to develop in the gas phases on either side of the membrane. Let's continue by assuming that initially the atmospheric composition on either side of the membrane is identical, and that the membrane initially exists as a non-porous barrier. Now, let's allow an evaporative surface on one side of the membrane to add H₂O molecules to the air, and let's add pores to the membrane. We will stipulate that the pore size must be of approximately the same dimension as the mean free path for air molecules (~ 1 μm in diameter); that is, the pores should be characterized by a high Knudsen number and they should facilitate Knudsen flow (see Section 5.B.3). In that condition, the pores will allow N₂ and O₂ molecules from the 'drier' side of the membrane to diffuse through the pores to the 'wetter' side of the membrane, and H₂O molecules

will diffuse in the opposite direction in partial compensation. However, because the diffusive flux of N_2 and O_2 will be greater than that of H_2O , the air pressure will increase on the 'wetter' side of the membrane. The small diameter of the pores will permit diffusive exchange, but not convective exchange; thus preserving pressure inequalities. If the air on the 'wetter' side of the membrane is open to a flow path with sufficiently low resistance, convective flow will occur. This mechanism of humidity-induced flow is most effective when pore sizes are small (Fig. 11.9). Pressure gradients can also develop on opposite sides of porous membranes in response to thermal gradients. Stomata tend to have pore diameters that are too large to foster Knudsen flow, except perhaps in the nearly closed state. There is evidence, however, that some wetland plants have channels between epidermal and palisade parenchyma cells that are of a smaller diameter (Dacey 1987). Observations of N_2/Ar ratios taken from gas inside leaves of the wetland plant *Nelumbo nucifera* revealed mass fractionation as a result of air diffusion across the leaf surfaces (Figure 11.10). The fractionation was less than that predicted by Graham's law, indicating that gas transport across the leaf was due to a combination of molecular diffusion and bulk flow. When calibrated against fractionation of N_2 and Ar after diffusion across synthetic nucleopore membranes, it was estimated that the leaf pores must be in the range 0.015-0.03 μm . The experiments were carried out under low light conditions. The nature of the pores is not known. Nonetheless, the observations provide evidence for the existence of pores capable of supporting Knudsen flow and the development of internal leaf pressure gradients through humidity-induced or thermal-induced diffusion.

The use of stable isotopes (especially $^{13}C/^{12}C$ ratios) has facilitated studies of the processes underlying CH_4 emissions to the atmosphere. Molecules transported purely by diffusion will fractionate according to Graham's Law. Molecules that are transported by convective bulk flow will not exhibit isotopic fractionation. This distinction can be used to investigate the contributions of each transport mechanism to CH_4 emissions to the atmosphere. Methane produced from SOM will possess molecules composed of either the ^{13}C or ^{12}C stable isotopes (some molecules will also be composed of ^{14}C , but we will ignore these for this example). The transport of CH_4 by diffusion alone will cause divergence in the $^{13}C/^{12}C$ ratio, which can be analyzed for CH_4 collected from the air spaces of leaves. As diffusion progresses, the CH_4 in leaves will become progressively more enriched in ^{13}C . If the principal transport mechanism to the atmosphere is bulk flow, then there should be no difference in the $^{13}C/^{12}C$ ratio of collected

CH₄. This experimental approach has been used to demonstrate the importance of both diffusive and convective processes in the overall CH₄ flux. In the case of rice, diffusion appears to be the dominant transport mechanism (Chanton and Whiting 1996, Chanton et al. 1997).

11.F The fluxes of nitrogen oxides from soils

The emission of nitrogen oxides (N_xO_x) from soils affects atmospheric processes in two important ways. First, nitrous oxide (N₂O) is a radiatively-active, greenhouse gas. Second, reactive nitrogen oxide compounds (collectively referred to as NO_x) support an active form of photochemistry that affects concentrations of atmospheric oxidants, such as ozone (O₃) and peroxyacyl nitrate (PAN). The NO_x compound that is emitted from soils in greatest abundance is nitric oxide (NO). The global emission rates of N₂O and NO have increased, along with the emission rates of CO₂ and CH₄, over the past century. Total global NO emissions from the surface to the atmosphere have been estimated to be 35-40 Tg N yr⁻¹; approximately 3-6 Tg N yr⁻¹ is due to emissions from natural ecosystems and 1-2 Tg N yr⁻¹ is from cropland ecosystems (Yan et al. 2005, Stehfest and Bouwman 2006, IPCC 2007). Another major source of NO_x emissions is biomass burning, which adds approximately 6 Tg N yr⁻¹, and the largest source overall is fossil fuel combustion, which adds approximately 25 Tg N yr⁻¹ (IPCC 2007).⁴ Total global N₂O emissions have been estimated to be 14 Tg N yr⁻¹; approximately 6 Tg N yr⁻¹ of which is from natural ecosystems and approximately 3.5 Tg N yr⁻¹ of which is from cultivated ecosystems (IPCC 2007). Production of N₂O from cultivated soils has increased in the past century, especially due to the increased use of ammonia-based fertilizers. The global industrial production of ammonia-based fertilizers increased from < 10 Tg N yr⁻¹ in 1950 to approximately 100 Tg N yr⁻¹ in 2008 (Erisman et al. 2008). Approximately 1% of the added nitrogen fertilizer is lost as N₂O (Stehfest and Bouwman 2006). Soils do not appear capable of assimilating N₂O at significant rates (Vieten et al. 2007), which is opposite to the case for CH₄. The atmospheric lifetime of N₂O is relatively long, at 120 years, and the largest natural sink, due to photochemical destruction in the stratosphere, is limited to 10-12 Tg N yr⁻¹ (Crutzen et al. 2007); thus the atmospheric concentration of N₂O has increased from approximately 270 nmol mol⁻¹ in 1750 to approximately 319 nmol mol⁻¹ in 2005 (IPCC 2007). The global warming potential for N₂O over a 100 year time frame is approximately 300 times higher than that of CO₂; due to its lower atmospheric concentration.

Most N₂O and NO fluxes originate from microbial nitrification and denitrification.

Nitrification is an aerobic process in which bacteria use NH₃ as an electron source and require O₂ as the ultimate respiratory electron acceptor. In soils, nitrification occurs through the serial activity of two groups of bacteria, the ammonia-oxidizing bacteria, principally in the genus *Nitrosomonas*, and nitrite-oxidizing bacteria, principally in the genus, *Nitrobacter*. The energetics of ammonia-to-nitrite oxidation, the first stage of serial nitrification is represented as:

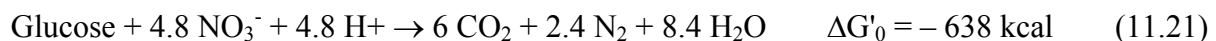


The second stage of nitrification involves the oxidation of NO₂⁻ to NO₃⁻:



The negative free energy change ($\Delta G'_0$) and positive reduction potential (E^0) are indicative of exergonic redox reactions (see Section 3.B). The energy-yielding electrons that nitrifying bacteria oxidatively strip from NH₃ are used to reduce CO₂, reflecting a form of autotrophic metabolism (similar in principle to photosynthetic autotrophic metabolism). During nitrification, some NO and N₂O is produced and emitted to the atmosphere, and the production of these products increases in anaerobic soils. These fluxes are small, however, compared to the fluxes that occur during denitrification.

Microbial *denitrification* occurs under anaerobic conditions. Denitrifying bacteria are able to respire anaerobically, replacing O₂, as the final electron acceptor, with NO₃⁻. The overall energetic balance of oxidizing glucose with NO₃⁻ as the final electron acceptor, compared to O₂, is quite similar:



Denitrification occurs in a series of steps (Fig. 11.11), with each step potentially carried out by the same or different specialist groups of bacteria or archaea. When considered as an entire pathway, the steps of denitrification convert soil NO₃⁻ to N₂, which is emitted to the atmosphere.

During the steps of denitrification and nitrification some molecules of NO and N₂O are known to 'leak' from pools in the pathway, causing a flux to the atmosphere. The amount of leakage has been shown to correlate positively with the overall availability of nitrogen and thus the overall activity of the nitrification and denitrification pathways. The ratio NO:N₂O in the leaked compounds has been negatively correlated with soil water content, which in turn influences soil O₂ content and compound diffusion rates (Davidson and Verchot 2000). It has been hypothesized that at high soil water content, the diffusion rate of NO from the nitrification pathway is reduced and the ratio of nitrification to denitrification shifts to favor denitrification. Both of these changes may force more NO through the microbial steps that favor its reduction to N₂O (Davidson et al. 2000). A conceptual model, known as the *hole-in-the-pipe model*, illustrates these controls over NO and N₂O emission rates, with the diameter of the pipe representing overall N flux through the pathways, and the diameter of the holes through which NO and N₂O leak representing control by soil water content (Fig. 11.12). The hole-in-the-pipe model has been important for organizing hypotheses about the controls over NO and N₂O emissions from soils. However, it is not quantitatively mechanistic and only loosely grounded in first-principles, such that it is limited as a tool for quantitative prediction.

Table 11.1. Fitted parameters for the general model presented by Chanzy and Bruckler (1993) for describing evaporation from bare soils.

Soil	a	b	c (s m⁻¹)
Loam	36.38	-3.61	-0.16
Silty clay loam	26.67	-4.06	-0.19
Clay	30.29	-7.52	-0.24

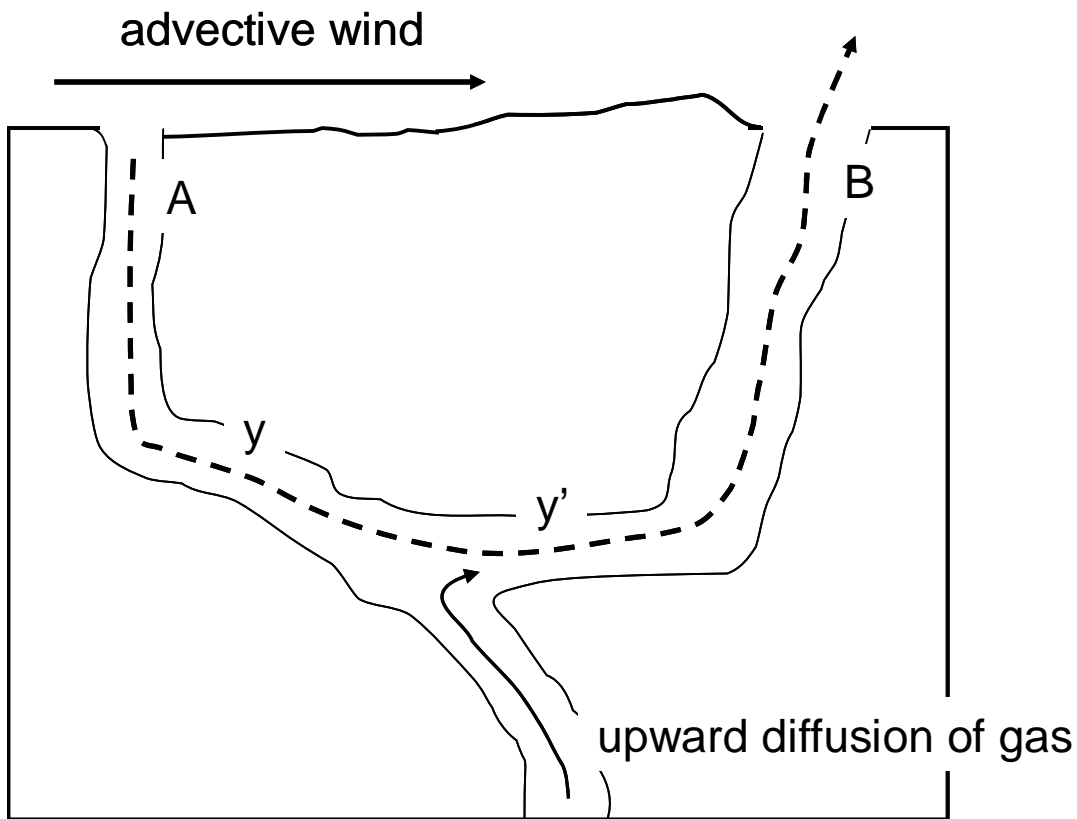


Figure 11.1. Microtopography of the soil surface in the presence of wind flow can cause pressure gradients within the soil pore system; leading to the phenomenon of ‘pressure pumping’. The pressure gradients can in turn drive the mass flow of an upward diffusing gas out of the soil. In this example, the small rise in topography from point A to point B, and connection of the points by a common channel within the soil causes a pressure gradient between points y and y’, which in turn forces the upward diffusing gas out of the soil at point B. Redrawn from a concept presented by Takle et al. (2004).

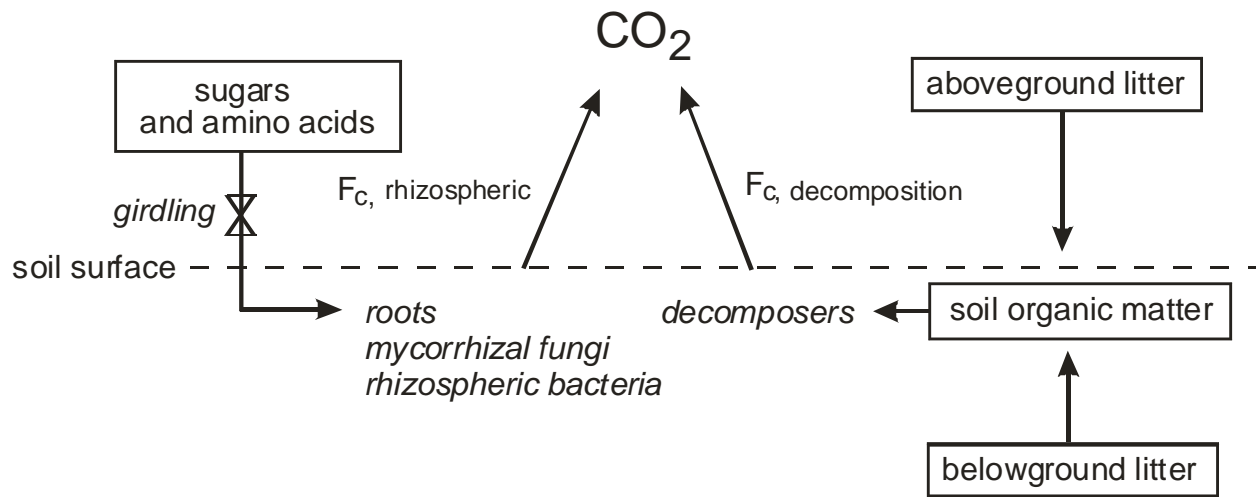


Figure 11.2. Partitioning of soil respiration into CO₂ fluxes due to rhizosphere-dependent organisms ($F_{c, \text{rhizospheric}}$) and decomposers ($F_{c, \text{decomposition}}$). The rhizosphere-dependent flux is supported by the downward transport of sugars and other substrates from the shoots of plants (often called rhizodeposition); this fraction can be eliminated by girdling the plants. The decomposition flux is supported by pools of soil organic matter derived primarily from litter inputs.

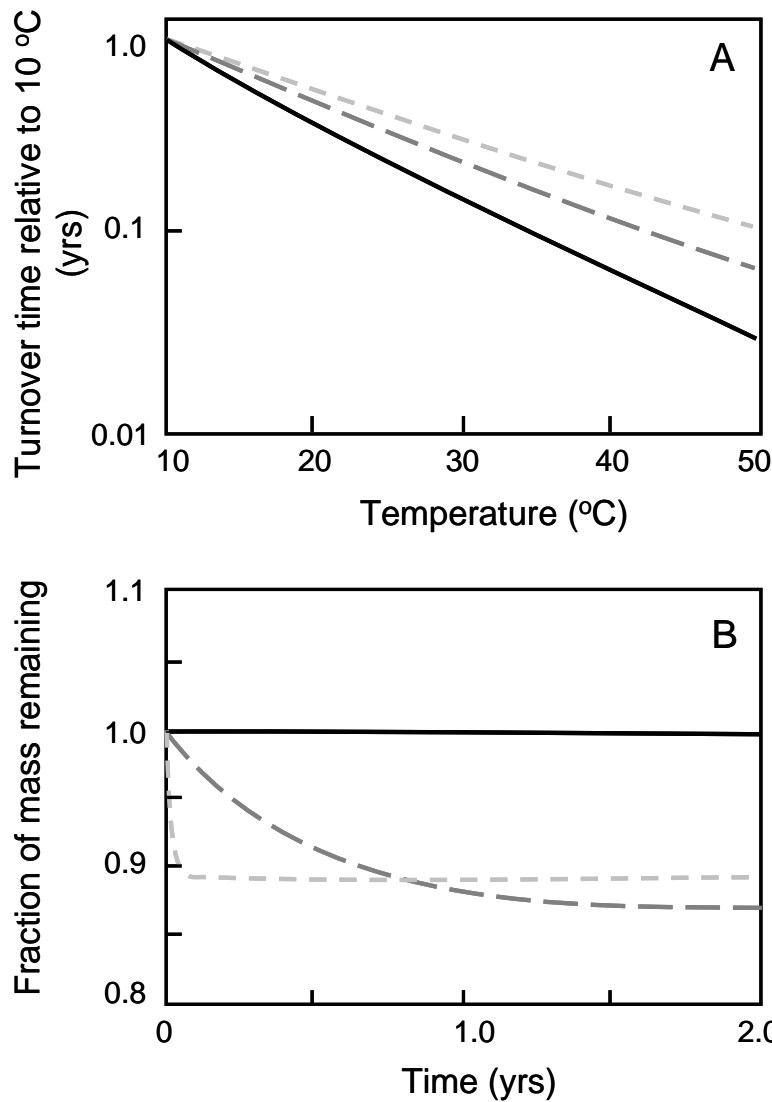


Figure 11.3. **A.** Modeled responses of turnover time in three SOM substrate pools: active (shown in light grey broken line), slow (shown in dark grey broken line) and passive (shown in black solid line) as a function of temperature. The results show that the passive pool is more sensitive to temperature increases than the slow and active pools. **B.** The fraction of mass lost due to decomposer respiration of each SOM substrate pool as a function of time following a step-wise increase in temperature of 2°C. Although the passive pool is more sensitive to temperature it turnover slowly due to its large size and recalcitrant nature. Redrawn from Knorr et al. (2005).

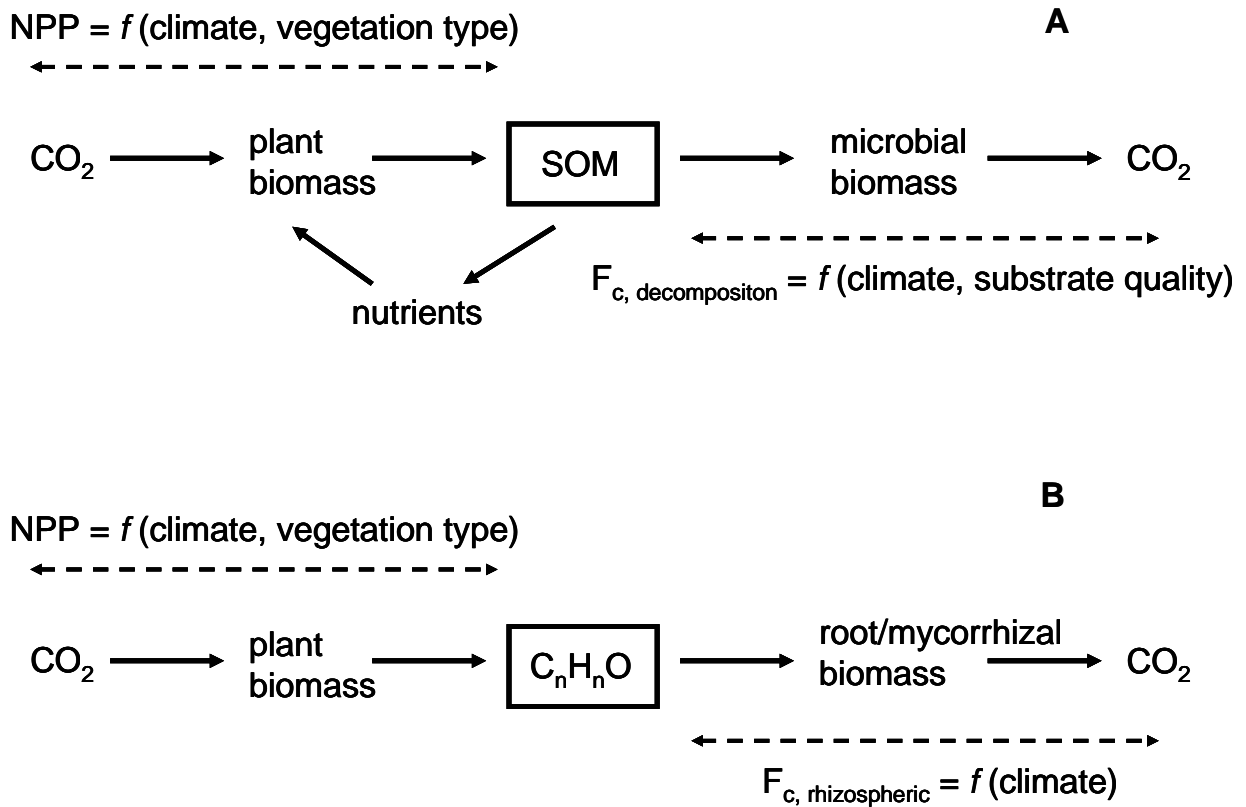


Figure 11.4. (A) General logic of heterotrophic soil respiration models recognizing that the heterotrophic component of the soil respiratory CO₂ flux ($F_{c, \text{decomposition}}$) is constrained by the input of litter from vegetation which is transformed into SOM from which soil microbes produce CO₂. (B) General logic of autotrophic soil respiration models recognizing that the rhizospheric component of the soil respiratory CO₂ flux ($F_{c, \text{rhizospheric}}$) is constrained by the availability of carbohydrate substrate (C_nH_nO) in the roots which serves as substrate for the respiratory metabolism of roots and mycorrhizal fungi.

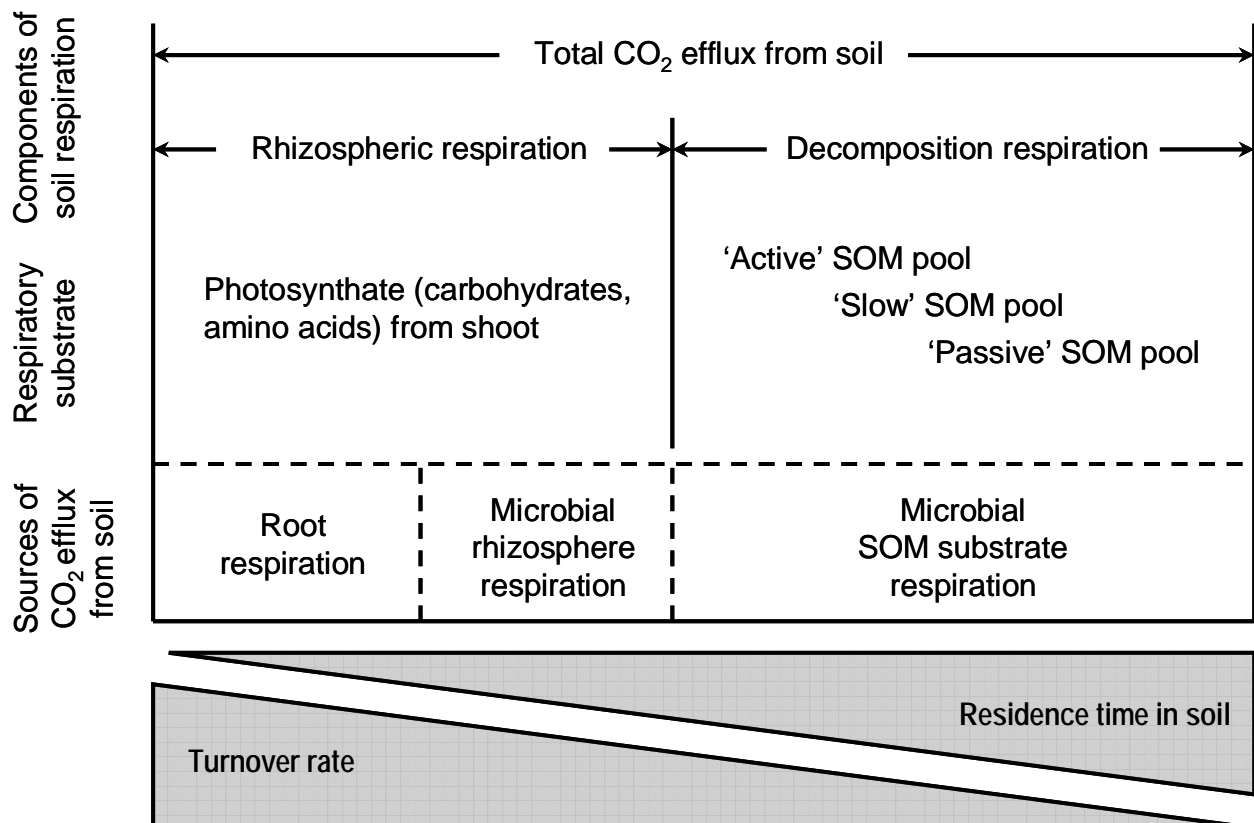


Figure 11.5. Scheme showing the components of soil respiration in relation to substrate type and CO₂ source. The transport of photosynthate from the shoot supports rhizospheric respiration with compounds that have a high turnover rate and short residence time in the soil. Decomposition respiration is derived from soil organic matter pools (SOM) that lower turnover rates and longer residence time. Modified from a concept presented in Kuzyakov 2006).

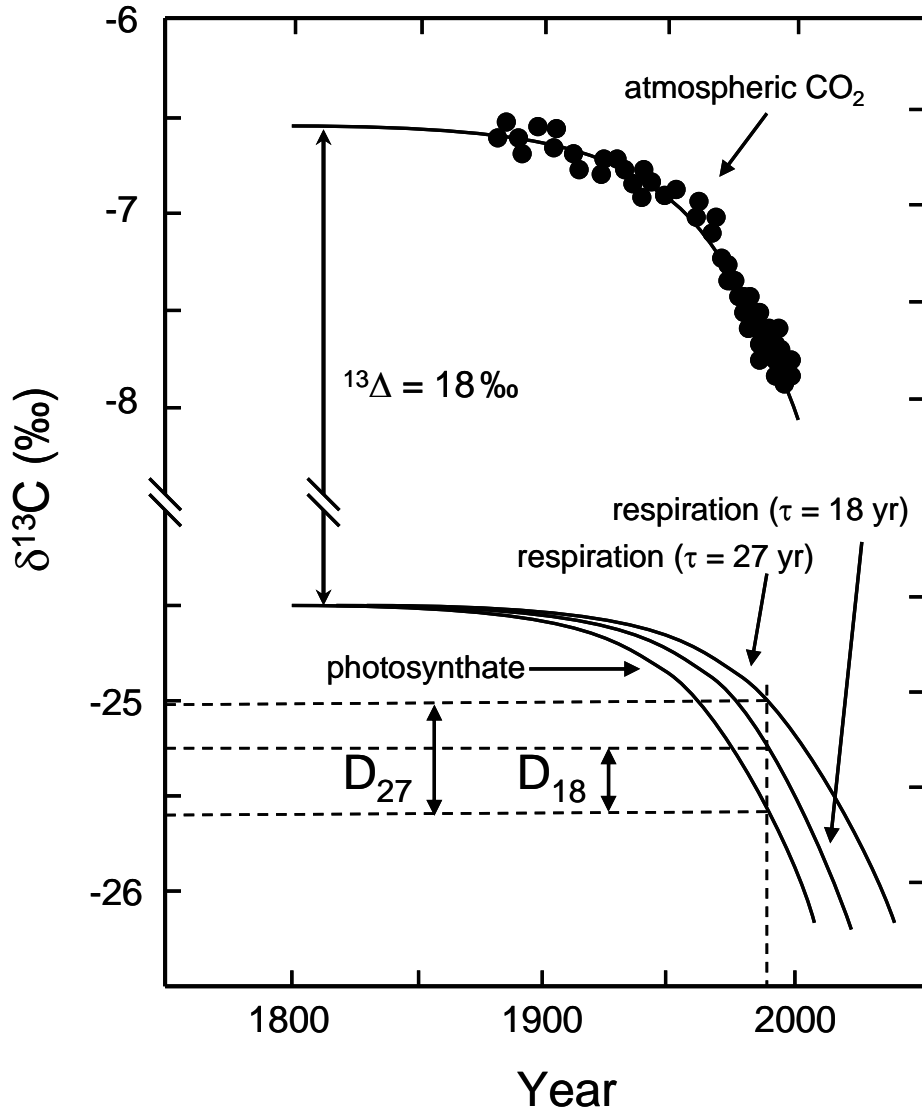


Figure 11.6. Graphic representation of the isotopic disequilibrium between the CO₂ assimilated by photosynthesis and emitted by soil respiration. The upper line and symbols (for the historical trend in the δ¹³C of atmospheric CO₂) is taken from Francey et al. (1999). We assume a photosynthetic discrimination of 18 ‰, from which we obtain an offset curve labeled here as 'photosynthate'. When the photosynthate curve is offset by 18 years or 27 years, representing estimates of the global mean residence time of assimilated CO₂, we obtain the curves labeled 'τ = 18 yr' and 'τ = 27 yr'. The global mean isotopic disequilibrium that occurs because respiration is offset by 18 or 27 years from photosynthesis is shown as D₁₈ and D₂₇, respectively. Redrawn from a concept presented by Yakir (2004).

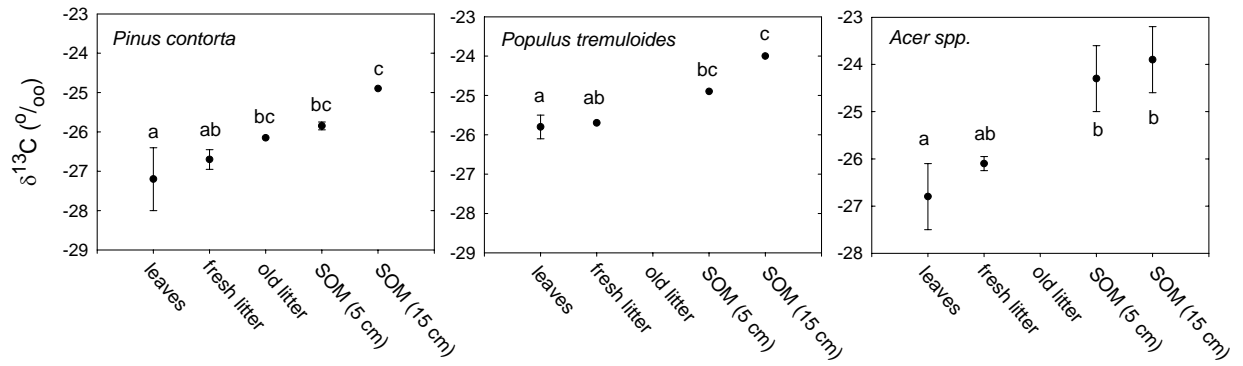


Figure 11.7. Enrichment in ^{13}C in soil litter and SOM at deeper layers of the soil profile in three ecosystems in northern Utah, USA. Vertical bars are ± 1 S.E. and points marked by different letters are statistically significant. Redrawn from Buchmann et al. (1997).

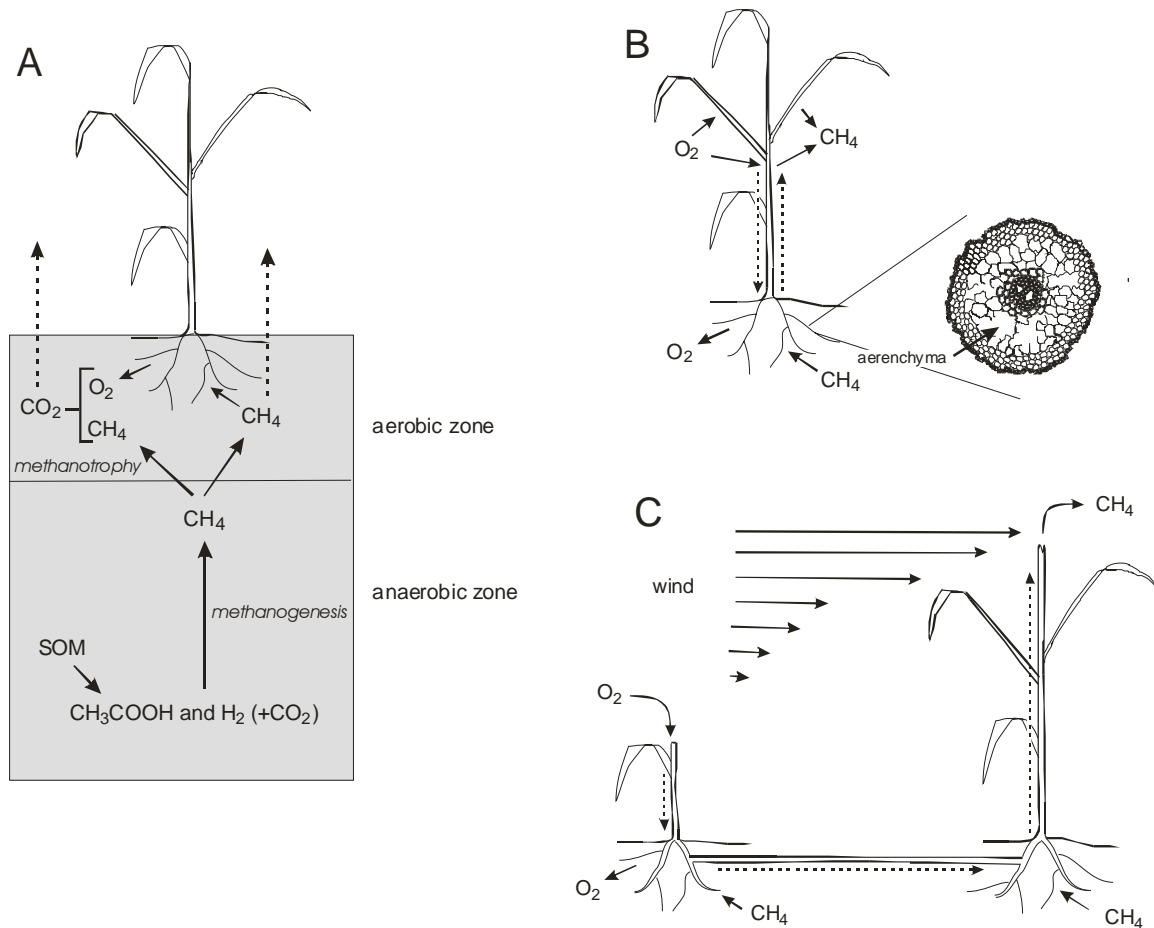


Figure 11.8. **A.** General scheme showing the location of methanogenesis and methanotrophy within the soil profile of a wetland system. **B.** Diffusion of O_2 (downward) and CH_4 (upward) through aerenchyma tissue in roots, stems and leaves of a wetland grass, *Spartina alterniflora*. The diffusive fluxes of these gases will follow their respective concentration gradients between the atmosphere and water-logged sediments. **C.** Advective transport of O_2 (downward) and CH_4 (upward) through broken stems of some wetland plants at different heights. Differential wind speed blowing across the canopy will create a pressure gradient that drives mass flow of air through connecting rhizomes between culms, thus creating a transport flow for O_2 and CH_4 .

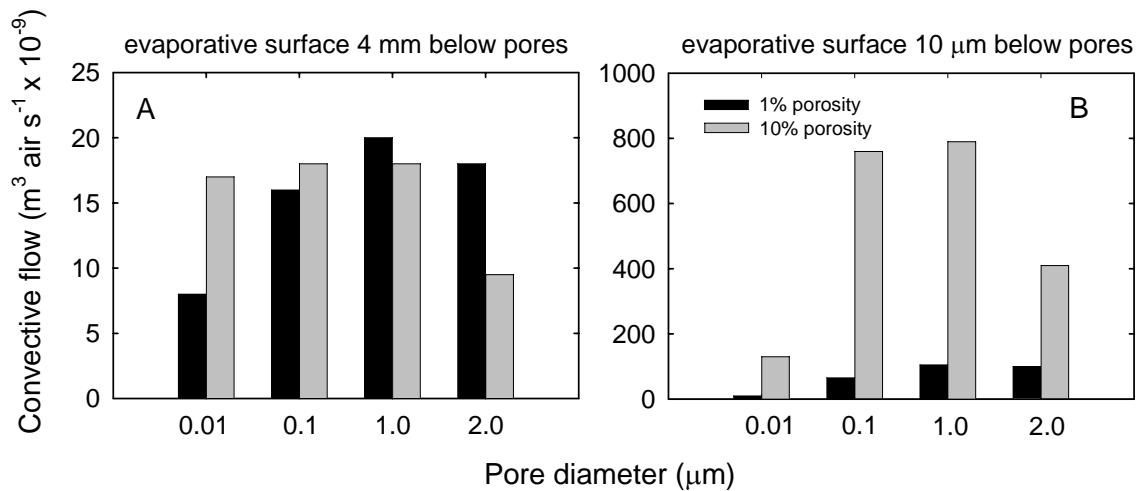


Figure 11.9. **A.** Modeled convective flow rate of air through a network of air channels potentially generated by humidity-induced mass flow. The diffusion of O₂ and N₂ through membrane pores of various diameters is assumed to occur in response to the humidity gradient formed on either side of the membrane by the presence of an evaporative surface 4 mm below one side of the membrane. Values were modeled for 1 % versus 10% pore area coverage in the membrane. **B.** Modeled convective flow for a system in which the evaporative surface is 10 μm below one side of the membrane. Note the difference in scale between panels A and B. Drawn from data presented in Armstrong et al. (1996).

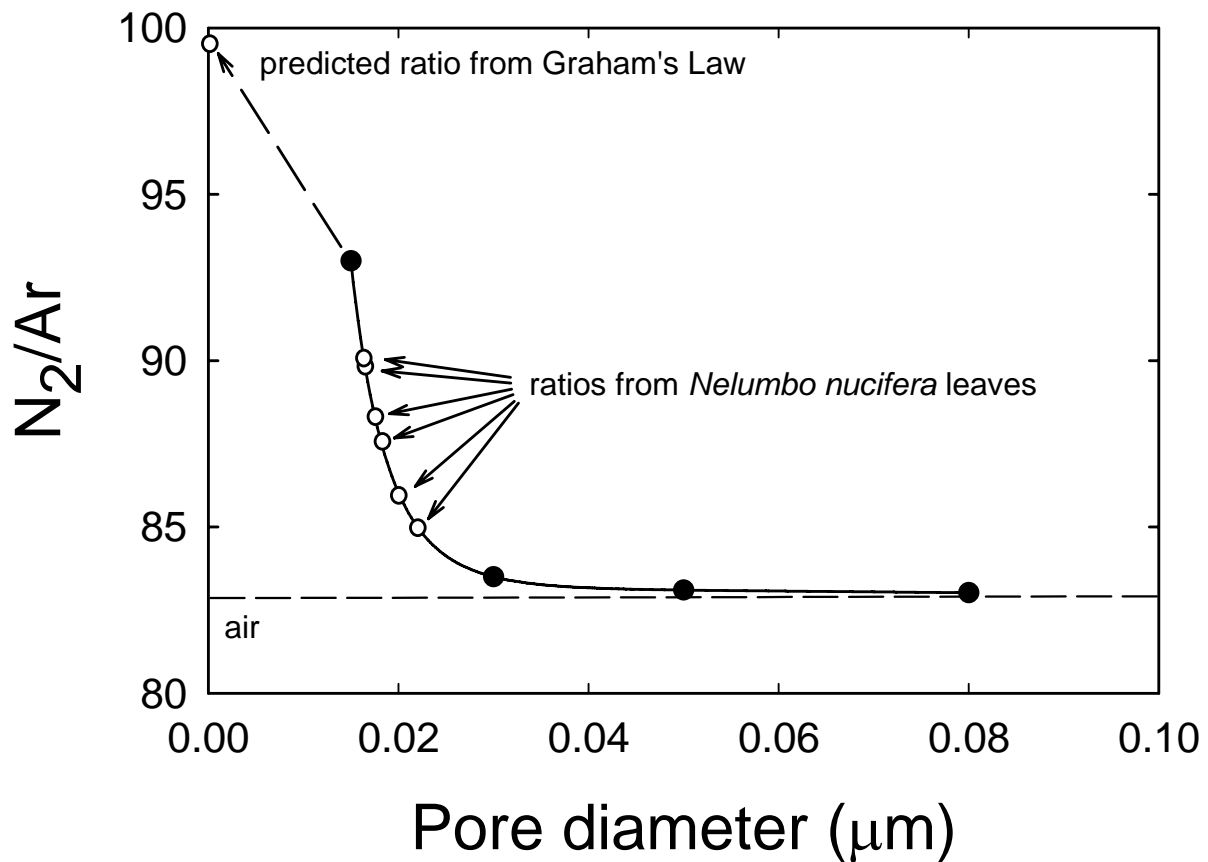


Figure 11.10. Relationship between pore size and observed nitrogen (N_2) to argon (Ar) ratios collected after air diffused through nucleopore membranes (solid circles) or the upper surface of leaves of the wetland species *Nelumbo nucifera* (open circles). The open circle on the y-axis represents the ratio (99.2) predicted by Graham's Law assuming pure molecular diffusion through a porous membrane. As pore size decreases, the ratio of Knudsen flow to bulk flow through the pores increases and mass fractionation occurs between the lighter compound Ar (mass 18) and the heavier compound N_2 (mass 28). Air naturally contains approximately 78% N_2 and 0.94% Ar. Gas collected from inside the leaves has N_2 /Ar ratios that are enriched in Ar relative to air, indicating that pore diameters in the leaf are in the range 0.015-0.03 μm , and thus likely to support Knudsen flow. These pores may facilitate pressurization of the internal leaf air spaces by humidity-induced or thermal-induced diffusion. Redrawn from Dacey (1987).

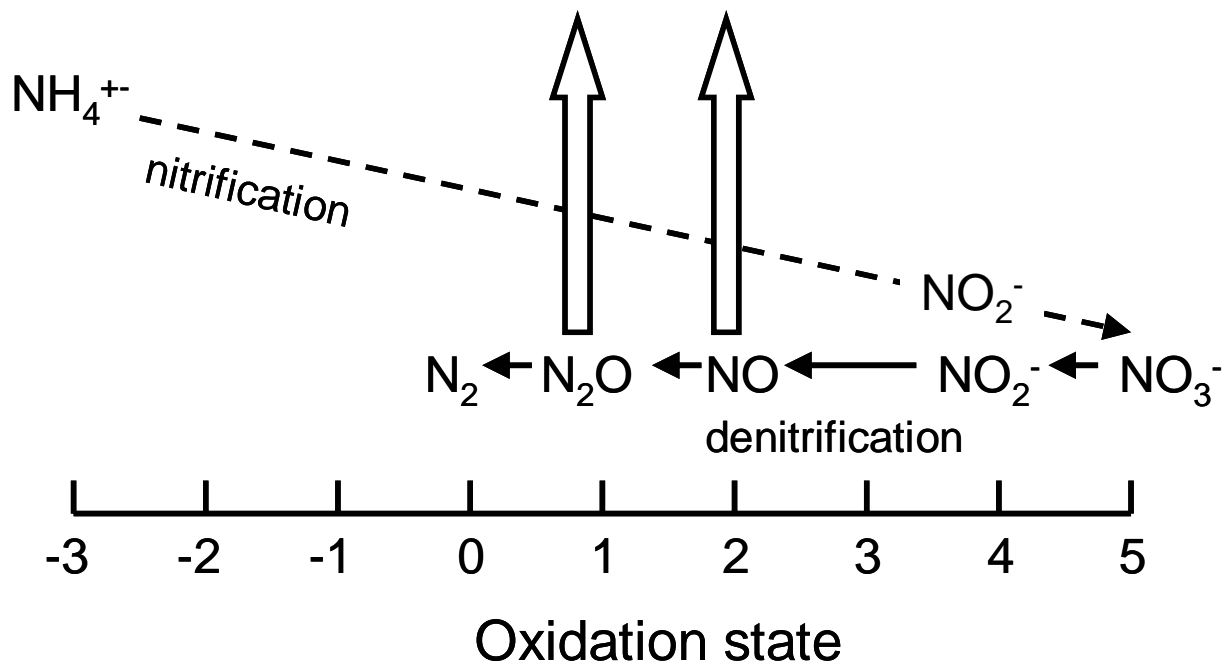


Figure 11.11. Schematic showing steps of nitrification and denitrification in relation to the oxidation state of nitrogen. The intermediate compounds NO and N_2O potentially leak from both pathways and enter the atmosphere.

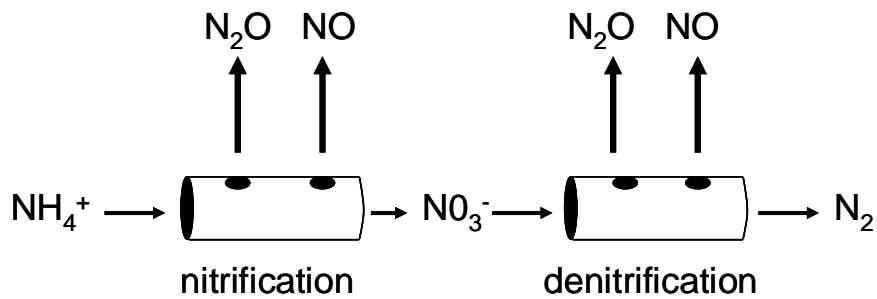


Figure 11.12. Hole-in-the-pipe conceptual model describing NO and N_2O fluxes from the nitrification and denitrification pathways. The flux rates are controlled by the amount of N compounds flowing through the pathways (pipes), and soil water content, which determines soil aeration. Based on a concept presented in Davidson et al. (2000).

Box 11.1 Photodegradation and decomposition

Plant litter exposed to bright sunshine exhibits mass loss during the exposure and higher rates of decomposition due to soil microorganisms compared to litter protected from sun exposure. This so-called *photodegradation*, has been principally attributed to the action of UV-B electromagnetic radiation (280-320 nm), although other wavebands can also be involved (Anesio et al. 1999, Brandt et al. 2009). Most of the lost mass is due to degradation of lignin, which is highly resistant to microbial decomposition (Henry et al. 2008). Photodegradation appears to be the source of direct emissions of carbon monoxide (CO) and CO₂ to the atmosphere (Tarr et al. 1995, Schade and Crutzen 1999, Brandt et al. 2009), and it has been shown to render lignin to be more susceptible to microbial decomposition once litter enters the pool of soil organic matter (Henry et al. 2008) (Figure B.11.1.1). Photodegradation has been shown to be especially important in the decomposition processes of arid ecosystems, where solar UV-B fluxes are high, and litter often remains on plants or the soil surface for relatively long periods of time prior to microbial decomposition (e.g., Austin and Vivanco 2006, Brandt et al. 2009). Photodegradation is dependent on exposure of litter surface area to UV radiation exposure, such that the basis on which we evaluate photodegradation is best referenced to litter surface area, rather than mass, as is typically done with regard to decomposition of soil organic matter. There is potential for species-specific differences in susceptibility to photodegradation, and this may be related to litter lignin content or other chemical aspects of the litter. There is still considerable work to be done to determine the principal controls and mechanisms that underlie photodegradation.

One issue that is likely to prove important involves potential direct and indirect interactions between photodegradation and microbial decomposition. As mentioned above, there is some evidence that the photochemical processing of lignin through photodegradation makes it more accessible for microbial decomposition once plant litter gets buried beneath the soil surface (Henry et al. 2008). However, any increase in the decomposability of lignin due to photodegradation would be balanced by the inhibitory effect of UV-B radiation on soil microbial biomass; thus, decreasing the decomposition potential of surface soils. These latter relations, in addition to the overall magnitude of photodegradation on soil carbon fluxes, remain to be elucidated.

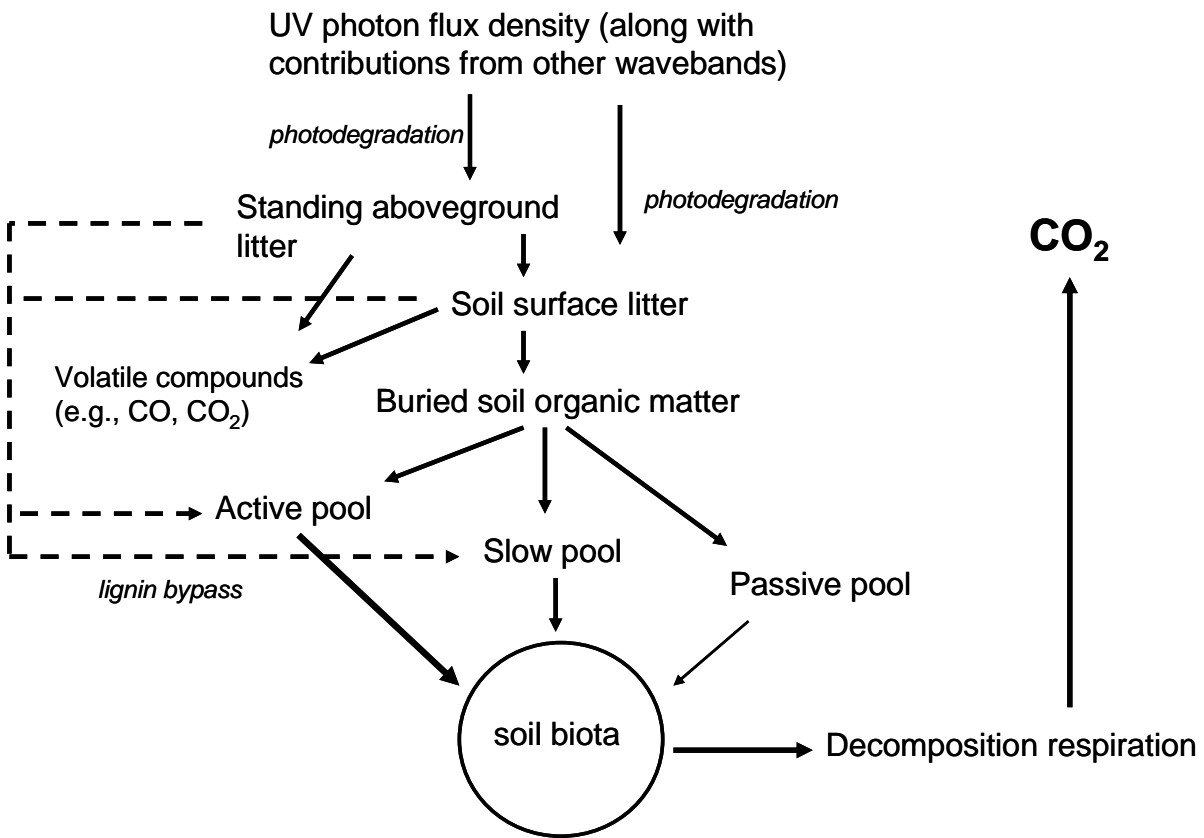


Figure B.11.1.1. Relations among processes and pools involved in the photodegradation of lignin and its subsequent decomposition as a component of soil organic matter.

Photodegradation causes chemical alteration of litter, resulting in the production of volatile products such as CO and CO₂, and it chemically transforms the litter in a way that enhances biotic decomposition from the various soil organic matter pools. The chemical transformation of litter is likely due to changes in lignin and/or to the priming of organisms capable of decomposing lignin, producing a 'lignin bypass' that may allow a larger fraction of lignin to enter the active and slow pools of soil organic matter and thus decompose more quickly.

Box 11.2 Modeling soil decomposition processes with biological realism

Some of the earliest models of litter decomposition highlighted the need for explicit recognition of different types of soil organisms and their differential roles in consuming and processing the various substrate pools obtained from soil organic matter (SOM) (Douce and Webb 1978, Smith 1979, Sinsabaugh et al. 1991). In some of these early models the microbial metabolism of organic substrates was described with various forms of the Michaelis-Menten model, which has been traditionally used to describe enzyme-substrate interactions (see Section 2.F). These early efforts provided a mechanistic perspective with which to model soil decomposition processes and laid the foundation for more explicit process-based models. As research efforts in ecosystem ecology began to merge with those in biogeochemistry, models of soil decomposition processes evolved to reflect progressively more biological insight (Parnas 1975, McGill et al. 1981, Moorhead and Sinsabaugh 2006). The foundational assumptions of these models are that microorganisms ultimately drive the decomposition process and that decomposition is proportional to microbial biomass and growth rate. As a general starting point, we can state that decomposition is a decay process, which means that the concentration of litter decreases over time. Assuming first-order kinetics in which decay rate is dependent on the concentration of organic matter substrates (c), we can write:

$$\frac{dc}{dt} = -kc \quad (\text{B.11.1.1})$$

where dc/dt is the molar loss of organic matter (per unit volume of soil) per day, and k is a rate coefficient, or turnover coefficient, with units days^{-1} . After integration, Equation B.6.1.1 can be used to calculate the amount of litter remaining after a given time interval (c_t) from the original organic matter concentration (c_0):

$$c_t = c_0 e^{-kt} \quad (\text{B.11.1.2})$$

Equation B.6.1.2 can be used to estimate SOM decomposition rates if the appropriate value for k is known. Past laboratory studies have estimated k as 0.2 d^{-1} for proteins (representative of the active SOM pool), 0.08 d^{-1} for cellulose and hemicellulose and 0.01 d^{-1} for lignin (with the latter

categories representative of the slow SOM pool, and even portions of the passive pool) (Paul and Clark 1989).

Deeper insight can be added to decomposition models if turnover is defined in terms of enzyme-substrate interactions and microbial diversity. Here, we will focus on the model developed by Moorhead and Sinsabaugh (2006), commonly called the Guild Decomposition Model (GDM), which in turn was influenced by theory developed in Sinsabaugh et al. (1991) and Schimel and Weintraub (2003). We can start with a general analogy:

$$\frac{dc}{dt} = -kc = -\frac{V_{\max}}{K_m + c} c \quad (\text{B.11.1.3})$$

In this case, the decay coefficient (k) is defined as $V_{\max}/(K_m + c)$, which places turnover time within the context of Michaelis-Menten kinetics. In this case, V_{\max} is defined with units mol (per unit volume soil) day⁻¹. In the original model derivations it was assumed that the principal control over decomposition is the activity of extracellular enzymes produced by microorganisms and that the concentration of litter and associated SOM is large compared to the concentration of extracellular enzymes (E). Under this condition, we can write:

$$\frac{dc}{dt} = -\frac{V_{\max}}{K_m + E} E \quad (\text{B.11.1.4})$$

Equation B.6.1.4 differs in form from typical Michaelis-Menten models in which the reaction rate is assumed to be limited by substrate concentration, rather than enzyme concentration. Equation B.6.1.4 can be expressed in terms of microbial biomass by assuming a fixed fraction of enzyme pool (a) to microbial biomass concentration (B), such that $E = a/B$, and defining K_m in terms of microbial biomass as $K_B = K_m/a$. Thus,

$$\frac{dc}{dt} = -\frac{V_{\max}}{K_B + B} B \quad (\text{B.11.1.5}).$$

Assuming that V_{\max} and K_B are constant for a particular soil with a stable community of microbial species, the dynamic variable in Equation B.6.1.5 is B; variations in B drive variations in decomposition rate. If we allow B to increase to extremely high values – i.e., the biomass concentration at which decomposition rate is no longer limited by B – then the decomposition rate will become zero-order with respect to B and first-order with respect to c. Under this condition K_B is small compared to B, and we can write:

$$\frac{dc}{dt} = -k_c c \approx -V_{\max} \quad (\text{B.11.1.6})$$

where the decay coefficient is now defined explicitly with respect to organic matter concentration (k_c). Alternatively, if we allow organic matter concentration (c) to increase to extremely high values, we can write:

$$\frac{dc}{dt} = -k_B B \approx -V_{\max} \quad (\text{B.11.1.7})$$

where the decay coefficient is defined with respect to microbial biomass concentration (k_B , also called r in some past model descriptions; e.g., Moorhead and Sinsabaugh 2006). Thus, when $B < k_c c / k_B$, we can write:

$$\frac{dc}{dt} = -\frac{k_c c B}{K_B + B} \quad (\text{B.11.1.8})$$

When $c < k_B B / k_c$, we can write:

$$\frac{dc}{dt} = -\frac{k_B B c}{K_C + c} \quad (\text{B.11.1.9})$$

where K_C is the Michaelis-Menten half-saturation coefficient with respect to organic matter concentration.

Moorhead and Sinsabaugh (2006) developed three microbial ‘guilds’ or functional groups according to: (1) opportunists that specialize on labile, water/ethanol soluble substrates principally through intracellular metabolism (highest growth rates), (2) cellulose/lignocellulose decomposers that use extracellular enzymes to degrade the largest fraction of litter biomass (moderate-to-slow growth rates), and (3) humus decomposers that degrade the most complex compounds in SOM (slow growth rates). Each of these guilds is assumed to specialize on one of three different sets of organic compounds: (1) soluble compounds (with concentration collectively represented as c_1), cellulosic compounds (c_2) and lignin (c_3). Thus, under the assumption that the size of each carbon pool limits the observed rate of decomposition, we can develop separate equations for each guild (i) and each set of compounds (j) with the generic form:

$$\frac{dc_j}{dt} = U_{ij} = \frac{k_{cij} B_i c_j}{K_{Cij} + c_j} \quad (\text{B.11.1.10})$$

Moorhead and Sinsabaugh (2006) took the modeling even further by considering (1) negative feedback on the decomposition of cellulose by lignin, and (2) perturbations to decomposition by nitrogen deposition from the atmosphere (which tends to stimulate the early stages of decomposition and inhibit the latter stages of decomposition). The feedback due to lignin is modeled by altering the K_C value, similar to modification of the K_m by competitive inhibitors in traditional Michaelis-Menten modeling. Modification of the K_C is justified by potential blockage of the active sites of extracellular enzymes that degrade cellulose (Sinsabaugh and Linkens 1989). In considering controls by nitrogen over decomposition, the nitrogen demand of the microbial biomass is determined as the difference between carbon uptake and respiration in relation to maintenance of a constant C:N ratio. Deposited N rectifies any gaps between demand and supply that might exist due to limited N mineralization rates, and controls increases or decreases in biomass accordingly. Any N that remains in excess of the growth demand by decomposing microbes is allowed to inhibit decomposition by the humus decomposing guild, which represents the late-stage decomposition that is most sensitive to excess N.

Box 11.3 Inferential statistical modeling: the example for soil respiration

Statistics is the science of information gathering, especially when the information arrives in little pieces instead of big ones.

Bradley Efron
Stanford University

Statistical analysis provides a means of organizing information about a process (or other type of phenomenon) into a quantitatively consistent model that can be used to predict the probability of a future outcome. Statistical models are a type of *empirically-based model* (see Section 1.D). Given the large amounts of data being generated by automated sensor networks distributed across the globe, statistical modeling has become an important prognostic activity in the earth system sciences. In this box, we highlight some of the common approaches taken in statistical modeling, and we use the modeling of soil respiration as an example by which to illustrate the overall approach.

Let's begin by assuming that we have access to a set of observations of soil respiration rate, which were made at different spots on the landscape and at different times during the growing season. We know that soil temperature is a principal controlling variable for the process, and our set of observations covers a broad range of soil temperatures. Thus, one obvious application of statistical modeling might involve organizing the observations into a statistical framework capable of predicting respiration rate from a given temperature. Using a classical inferential approach, we might develop a statistical regression with soil temperature represented as the independent variable and soil respiration rate as the dependent variable. We can then estimate the best-fit mathematical function to describe the relation; we refer to that function as our *process model*. Most likely, the model will be some type of exponential relation with a specified slope and y-intercept, which we refer to as *model parameters*. An assumption implicit in the analysis is that our method has *optimized* the model parameters given the condition of the observed data. In formal terms, we are predicting the *joint probability distribution* of a dependent variable (y) and a covariate (x):

$$y_i = \beta_0 + e^{\beta_1 x_i} + \varepsilon_i \quad (\text{B.11.3.1})$$

where y_i and x_i are the variables associated with independent observation i , β_0 and β_1 are the intercept and slope parameters in the model, respectively, and ε_i is the error referenced to observation i .

Now, having conducted this exercise, we assume that there is some level of uncertainty in the model parameters. The data we have collected are likely to provide an imperfect picture of the true relation between temperature and respiration rate. If we had assembled a different mix of observation days or measurement spots, we would have derived slightly different parameters. Thus, much of the uncertainty resides in the fact that we have randomly chosen the set of data on which to base the model. We can use hierarchical, mixed effects statistical approaches to partition the random effects in the observations, and thus quantify the uncertainty. In fact, if we want to control for these effects, we can create an even more complex model and include these effects as additional parameters. This type of exercise would fall completely within the realm of *classical statistics*.

In recent years, it has become popular to deploy a second type of statistical inference known as *Bayesian analysis*. Bayesian analysis takes advantage of *prior knowledge* in shaping an initial estimate of model parameters. We then use the observations we have collected to 'hone' our initial estimate of the parameters. Prior knowledge about the distribution of a parameter (or set of parameters) can narrow the range of parameter estimates that are permitted and thus decrease uncertainty. Let's return to our example of soil respiration rate. Let's assume that we want to explore more fully the uncertainty in one parameter of the model, the slope of the regression; referred to here as β_1 . If we treat temperature as a fixed covariate – in other words, we assume it is measured and prescribed as an explicit value in the model – we can focus the analysis on the relationship between β_1 and the data that we've collected. In Bayesian terms, we would represent the parameter estimation process as:

$$p(\beta_1, \text{model} \mid \text{data}) \propto p(\text{data} \mid \text{model}, \beta_1) p(\text{model} \mid \beta_1) p(\beta_1) \quad (\text{B.11.3.2})$$

We can state Equation B.11.3.2 in words as: 'the joint probability distribution of β_1 and the model, given the observed data, is proportional to the probability of the data, given the model and β_1 , multiplied by the probability of the model, given β_1 , multiplied by the probability of β_1 '.

Working from the right to the left, Equation B.11.3.2 states that: (1) if we have an estimate of the distribution of β_1 , (2) if we know how the model responds to that distribution, and (3) if we can come up with a way to determine how the data compare to the model output using our estimated distribution of β_1 , then (4) we can use the data to improve our initial estimate of the distribution of β_1 . In order for Bayesian analysis to be most effective we should have access to both prior knowledge about the distribution of a parameter *and* a model that is dependent on the parameter. The aim of formulating Equation B.11.3.2 is to 'explore the parameter space' and determine the optimum estimate for the parameter(s); by optimum we mean the value of β_1 that provides the least error between the modeled data and observed data.

How do we find the parameter optimum? We begin with our previous knowledge about the distribution of β_1 , which we will call our *prior parameter distribution*, and designate it as $p(\beta_1)$ (see Fig. 11.3.1). We then sample values of β_1 from that prior distribution using a random sampling protocol; i.e., techniques such as Monte Carlo Markov Chain (MCMC) sampling or Gibbs sampling are often used. We enter these sampled values of β_1 into our model and predict a set of values that can be compared to the observed values. A *merit function*, such as maximum likelihood, is then used to evaluate the total error between the sets of predicted and observed values. This error is often called the *model-data mismatch*. The mismatch will be initially high, but using feedback between the merit and sampling functions, the sampled range of β_1 is progressively narrowed. Eventually, a set of parameter values is obtained which provide approximately equal amounts of model-data error. Through the numerous iterations (often numbering thousands) during which the sampling program is randomly choosing values of β_1 , and given that the sampled range of β_1 narrows with each successive iteration, multiple selections of the same β_1 values will occur, and the frequency by which the program samples each value of β_1 can be represented as a probability distribution. The ultimate probability distribution that emerges from the process is called the *posterior parameter distribution*. Provided that the data provides adequate constraint on the parameter estimation, the posterior distribution will be narrower than the prior distribution. An optimal value for β_1 can be selected from the peak of the posterior distribution and formal estimates of uncertainty can be generated from the distribution tails on either side of that peak.

This is just one example of how Bayesian techniques can be applied to flux data. We will consider the process again in the chapter on turbulent (eddy) fluxes as a useful means to inform ecosystem process models. In that case, multiple parameters from complex models can be estimated and optimized simultaneously. More detailed discussions of statistical aspects of the topic are presented in Clark and Gelfand (2006), Ogle and Barber (2008), and Cressie et al. (2009).

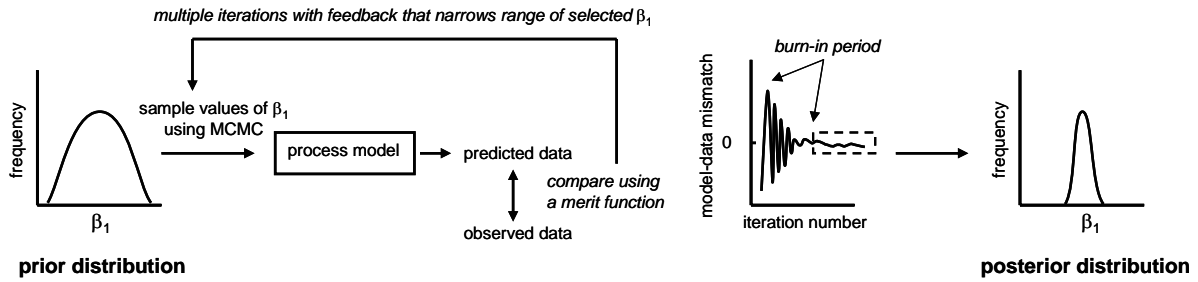


Figure B.11.3.1. Scheme showing steps taken in a Bayesian process whereby estimates of parameter values for a representative process model are optimized and uncertainties reduced in producing a posterior parameter distribution from a prior (estimated distribution).

Footnotes Chapter 11

¹ The enrichment of atmospheric CO₂ above a canopy in ¹³C during the day is often obscured by atmospheric mixing; but is clearly observed during daylight hours when turbulent mixing is low, such as in the morning.

² Parenthetical words added by authors for clarity.

³ Here, we make a distinction between convection and advection in that convection is driven by two component processes in parallel, molecular diffusion and bulk-flow due to pressure gradients, whereas advection is used to describe only pressure-driven bulk flows.

⁴ The emission of NO to the atmosphere due to fossil fuel combustion originates from the oxidation of N contaminants in coal, for example, and O₂ thermolysis through the Zeldovich mechanism which occurs at temperatures of approximately 2000 K and higher: $O_2 \leftrightarrow O + O$, $O + N_2 \leftrightarrow NO + N$, $N + O_2 \leftrightarrow NO + O$.